

On the Design of Modular Reflecting *EM* Skins for Enhanced Urban Wireless Coverage

P. Rocca,⁽¹⁾⁽²⁾ *Senior Member, IEEE*, P. Da Rú,⁽¹⁾ N. Anselmi,⁽¹⁾ *Member, IEEE*, M. Salucci,⁽¹⁾ *Member, IEEE*, G. Oliveri,⁽¹⁾ *Senior Member, IEEE*, D. Erricolo,⁽⁴⁾ *Fellow, IEEE*, and A. Massa,⁽¹⁾⁽³⁾⁽⁵⁾ *Fellow, IEEE*

⁽¹⁾ *ELEDIA Research Center (ELEDIA@UniTN - University of Trento)*

DICAM - Department of Civil, Environmental, and Mechanical Engineering

Via Mesiano 77, 38123 Trento - Italy

E-mail: {*paolo.rocca, pietro.daru, nicola.anselmi, marco.salucci, giacomo.oliveri, andrea.massa*}@unitn.it

Website: www.eledia.org/eledia-unitn

⁽²⁾ *ELEDIA Research Center (ELEDIA@XIDIAN - Xidian University)*

P.O. Box 191, No.2 South Tabai Road, 710071 Xi'an, Shaanxi Province - China

E-mail: *paolo.rocca@xidian.edu.cn*

Website: www.eledia.org/eledia-xidian

⁽³⁾ *ELEDIA Research Center (ELEDIA@UESTC - UESTC)*

School of Electronic Engineering, Chengdu 611731 - China

E-mail: *andrea.massa@uestc.edu.cn*

Website: www.eledia.org/eledia-uestc

⁽⁴⁾ *Andrew Electromagnetics Laboratory - University of Illinois Chicago*

Department of Electrical and Computer Engineering, 851 South Morgan Street, Chicago, IL 60607-7053 - USA

E-mail: *derrickl@uic.edu*

Website: <https://andrew.lab.uic.edu/>

⁽⁵⁾ *ELEDIA Research Center (ELEDIA@TSINGHUA - Tsinghua University)*

30 Shuangqing Rd, 100084 Haidian, Beijing - China

E-mail: *andrea.massa@tsinghua.edu.cn*

Website: www.eledia.org/eledia-tsinghua

This work has been submitted to the IEEE for possible publication. Copyright may be transferred without notice, after which this version may no longer be accessible.

On the Design of Modular Reflecting *EM* Skins for Enhanced Urban Wireless Coverage

P. Rocca, P. Da R  , N. Anselmi, M. Salucci, G. Oliveri, D. Erricolo, and A. Massa

Abstract

The design of modular, passive, and static artificial metasurfaces to be used as electromagnetic skins (*EMS*s) of buildings for improving the coverage in urban millimeter-wave communication scenarios is addressed. Towards this end, an *ad-hoc* design strategy is presented to determine optimal trade-off implementative solutions that assure a suitable coverage of the areas of interest, where the signal from the base station is too weak, with the minimum complexity. More specifically, the admissible surface in the building facade is first partitioned into tiles, which are the minimum-size elements of the artificial coating (i.e., the building block of an *EMS*). Then, the search for the optimal *EMS* layout (i.e., the minimum number and the positions of the tiles to be installed) is carried out with a binary multi-objective optimization method. Representative numerical results are reported and discussed to point out the features and the potentialities of the *EMS* solution in the smart electromagnetic environment (*SEME*) as well as the effectiveness of the proposed design method.

Key words: Smart EM Environment, Artificial Materials, Mobile Communications, Millimeter-wave, Multi-Objective Optimization.

1 Introduction

Starting from the first generation of cellular networks, back when the communications were analog and the portable devices heavy and cumbersome, there has always been a continuous technological push towards higher data rates, which are a mandatory requirement with the introduction of smart-phones and the sharing of multimedia contents now enabled by the fast and reliable data streams of 4G and 5G communication networks [1]-[3]. Regardless of the throughput of modern communication networks, the data traffic is expected to further increase in the next years because of the massive proliferation of wireless devices and systems (e.g., smart-phones, tablets, internet-of-things (*IoT*) sensors, and robots) as well as the introduction of novel applications including, for instance, the autonomous driving [4], the tactile internet [5], and the remote control of robots [6]. All these applications will unavoidably require improved coverage (i.e., a higher level of the *EM* signal in the coverage area) and better quality-of-service (*QoS*) for mobile users/devices as well as wireless links characterized by lower latency and higher throughput/resiliency [7][8]. Towards this end, future mobile communication networks will have to assure more and more reliable and ubiquitous connections, everywhere and any-time, as never seen before. However, the standard solutions chosen by the operators (i.e., installing more base stations (*BSs*), transmitting more power, or using new frequency bands) are no longer applicable because of the too high power consumption due to the foreseen explosion of the traffic needs as well as the spectrum congestion [9]. Moreover, the obstacles/scatterers in the environment cannot be neglected due to the increase in the operation frequencies (e.g., millimeter-waves in 5G [10]) so that the no line-of-sight (*NLOS*) condition has to be taken into account since the design of the wireless network architecture.

A possible countermeasure to these issues and challenges is the “implementation” of the so-called smart electromagnetic environment (*SEME*) [11], where the objects and the scatterers within the environment are considered, unlike the past, as enablers [12] of the electromagnetic (*EM*) propagation and not impairments. The environment is thus exploited as an additional degree-of-freedom (*DoF*) for tailoring the propagation of the *EM* waves and to enhance the signal strength in the “blind spots”, namely the zones where the signal from the base station is too weak to support a desired throughput for users’ applications [12]. By using artificial ma-

materials (e.g., engineered materials or metamaterials [13]) on the building facades or integrated within panels along the streets, the propagation of the *EM* waves in complex urban scenarios is controlled to fit *QoS* requirements and coverage targets. Passive (i.e., without active amplifiers) reconfigurable metasurfaces, which behave like intelligent reflecting surfaces (*IRSs*) [14]-[20] thanks to simple electronic devices such as radio-frequency switches [21], have been successfully installed, but they will not be massively deployed until their cost is significantly reduced. An opposite strategy still profitably exploits the objects in the environment, without introducing additional materials, but optimizing the excitations of the array elements of the *BS* to generate a desired *EM* field distribution in the desired spots [22]. Although there are no additional costs and an installation of new hardware is not required, the opportunistic use of the *BS* array offers to the designer a limited number of *DoFs* and an accurate knowledge of the surrounding scenario is also needed to assure a suitable/stable *QoS*.

Differently, this paper is concerned with the instance of the *SEME* vision aimed at providing a doable large-scale solution suitable for the mass production. More specifically, it proposes a method for the design of modular, passive, and static metasurfaces to build effective and low-cost *EMSs*. In telecommunication engineering, the term *EMS* refers to a device conformal to the external surface of the object, where it is installed, that offers a set of functionalities related to the sensing and the manipulation of the *EM* waves [23]. A typical deployment for an *EMS* is over the facades of a building, which are strategic assets in a urban scenario for redirecting the impinging *EM* field towards areas where the signal would otherwise be weak. Starting from the selection/definition of the maximal area available on a building facade, the support of the *EMS* is discretized into tiles, which are the elementary building blocks of an *EMS*. The arrangement of the tiles on the admissible surface of the facade is then optimized with a multi-objective global optimization strategy based on a binary implementation of the Non-Dominated Sorting Genetic Algorithm II (*NSGA-II*) [24] to yield the optimal trade-off solutions between the best coverage of the zones of interest and the minimum number of tiles.

To the best of the authors' knowledge, the main innovative contributions of this research work include (i) the description, the statement, and the mathematical formalization of a novel design problem within the *SEME* framework, (ii) the development of a customized design strategy for

selecting the minimum number of tiles of the *EMS* that assures the coverage of the regions of interest, and (iii) the synthesis of innovative tiled *EMS*s to be embedded in the facade of buildings for improving the *EM* coverage within urban millimeter-wave communication scenarios.

The rest of the paper is organized as follows. The synthesis problem of the modular, passive, and static *EMS* is mathematically described and formulated in Sect. 2, while the optimization-based design method is presented in Sect. 3. Section 4 deals with the validation and the numerical assessment of the proposed concepts and synthesis method by considering realistic urban scenarios served by a millimeter-wave band of 5G systems. Eventually, some conclusions and final remarks are drawn (Sect. 5).

2 Mathematical Formulation

Let us consider an urban scenario [Fig. 1(a)] where a *BS* serves the terminals and the devices in the surrounding environment to implement the communication network by providing wireless services to the users with a suitable *QoS*. Because of the presence and the configuration of the buildings, the signal from the *BS* is absent or too weak to guarantee a connection to the network or a sufficient throughput in some areas, $\{\Omega_b; b = 1, \dots, B\}$, of the scenario at hand. In order to increase the signal strength in these “blind spots”, the installation of artificial *EMS*s is considered.

For the sake of formulation simplicity, the case of a single “blind spot” (i.e., $B = 1, \Omega \leftarrow \Omega_b$), where there is neither direct nor reflected signal from the *BS*, and the design of a single *EMS* on a facade of a building is considered in this work. However, it is worthwhile pointing out that both the theoretical description and the proposed design method can be straightforwardly extended to the case with multiple skins over multiple buildings to cover multiple blind spots. With reference to such a benchmark, an area \mathcal{S} on the external wall of a selected building is assumed to be located on the $y - z$ plane, subdivided into N square tiles, $\{\mathcal{S}^{(n)}; n = 1, \dots, N\}$ ($\bigcup_{n=1}^N \mathcal{S}^{(n)} = \mathcal{S}$), of equal size $\Delta\mathcal{S}$ ($\Delta\mathcal{S} = L \times L$, L being the side length of each tile), and centered at the positions $\mathbf{r}_S^{(n)} = y_S^{(n)}\hat{\mathbf{y}} + z_S^{(n)}\hat{\mathbf{z}}$ ($n = 1, \dots, N$) [Fig. 1(b)], while the *BS* is located at $\mathbf{r}_{BS} = x_{BS}\hat{\mathbf{x}} + y_{BS}\hat{\mathbf{y}} + z_{BS}\hat{\mathbf{z}}$ in the far-field of \mathcal{S} .

Without loss of generality, the *EM* wave generated from the *BS* and impinging on the *EMS* is

modeled as a monochromatic plane wave at the working frequency f with electric field [25][26]

$$\mathbf{E}_{\mathfrak{S}}(\mathbf{r}) \triangleq E_{\mathfrak{S}} \hat{\mathbf{e}}_{\mathfrak{S}} e^{-jk_{\mathfrak{S}} \cdot (\mathbf{r} - \mathbf{r}_S^{(0)})} \quad (1)$$

where $E_{\mathfrak{S}}$ is the complex-valued wave amplitude, $\hat{\mathbf{e}}_{\mathfrak{S}}$ is the complex polarization vector, and $\mathbf{k}_{\mathfrak{S}}$ ($\mathbf{k}_{\mathfrak{S}} \triangleq -k [\sin \theta_{\mathfrak{S}} \cos \phi_{\mathfrak{S}} \hat{\mathbf{x}} + \sin \theta_{\mathfrak{S}} \sin \phi_{\mathfrak{S}} \hat{\mathbf{y}} + \cos \theta_{\mathfrak{S}} \hat{\mathbf{z}}]$) is the incident wave vector, k being the free-space wavenumber ($k \triangleq \frac{2\pi}{\lambda}$, λ being the wavelength at f), while $(\theta_{\mathfrak{S}}^{(0)}, \phi_{\mathfrak{S}}^{(0)})$ is the direction of arrival of the incident wave from the BS to the center of \mathcal{S} , $\mathbf{r}_S^{(0)}$ ($\mathbf{r}_S^{(0)} = y_S^{(0)} \hat{\mathbf{y}} + z_S^{(0)} \hat{\mathbf{z}}$) [Fig. 1(b)], being $\theta_{\mathfrak{S}}^{(n)} \Big|_{n=0} = \arccos \left(\frac{z_{BS} - z_S^{(n)}}{|\mathbf{r}_{BS} - \mathbf{r}_S^{(n)}|} \right) \Big|_{n=0}$ and $\phi_{\mathfrak{S}}^{(n)} \Big|_{n=0} = \arctan \left(\frac{y_{BS} - y_S^{(n)}}{x_{BS} - x_S^{(n)}} \right) \Big|_{n=0} = \arctan \left(\frac{y_{BS} - y_S^{(n)}}{x_{BS}} \right) \Big|_{n=0}$ since $x_S^{(0)} = 0$.

Each tile $\mathcal{S}^{(n)}$ ($n = 1, \dots, N$) of the EMS is illuminated from the direction $(\theta_{\mathfrak{S}}^{(n)}, \phi_{\mathfrak{S}}^{(n)})$ and it reflects the impinging wave towards the direction $(\theta_{\mathfrak{R}}^{(n)}, \phi_{\mathfrak{R}}^{(n)})$ [$\theta_{\mathfrak{R}}^{(n)} = \arccos \left(\frac{z_{\Omega}^{(n)} - z_S^{(0)}}{|\mathbf{r}_{\Omega}^{(n)} - \mathbf{r}_S^{(0)}|} \right)$, $\phi_{\mathfrak{R}}^{(n)} = \arctan \left(\frac{y_{\Omega}^{(n)} - y_S^{(0)}}{x_{\Omega}^{(n)}} \right)$] by focusing the reflected beam in the point $\mathbf{r}_{\Omega}^{(n)}$ ($\mathbf{r}_{\Omega}^{(n)} = x_{\Omega}^{(n)} \hat{\mathbf{x}} + y_{\Omega}^{(n)} \hat{\mathbf{y}} + z_{\Omega}^{(n)} \hat{\mathbf{z}}$) of the coverage region Ω , which is also called area of interest (AoI). More in detail, the AoI is assumed parallel to the $x - y$ plane (i.e., $z_{\Omega}^{(n)} = z_{\Omega}$, $\forall n$), centered at $\mathbf{r}_{\Omega}^{(0)}$, and discretized into N partitions, $\{\Omega^{(n)}; n = 1, \dots, N\}$ (i.e., $\bigcup_{n=1}^N \Omega^{(n)} = \Omega$), located at $\mathbf{r}_{\Omega}^{(n)}$ ($n = 1, \dots, N$) with equal dimensions $\Delta\Omega^{(n)} = \Delta\Omega$ [Fig. 1(b)].

By neglecting the polarization and the reflection losses, the far-field expression of the electric field reflected from the n -th ($n = 1, \dots, N$) tile $\mathcal{S}^{(n)}$ in a generic point $\tilde{\mathbf{r}}$ of the local coordinate system⁽¹⁾ (Fig. 2), $\mathbf{E}_{\mathfrak{R}}^{(n)}(\tilde{\mathbf{r}}) = E_{\mathfrak{R}}^{(n)}(\tilde{\mathbf{r}}) \hat{\mathbf{e}}_{\mathfrak{R}}$, is given by the following closed-form expression [29]

$$E_{\mathfrak{R}}^{(n)}(\tilde{\mathbf{r}}) \simeq -jk\eta \frac{e^{-jk(d_{\mathfrak{S}}^{(n)} + d_{\mathfrak{R}}^{(n)})}}{4\pi d_{\mathfrak{S}}^{(n)} d_{\mathfrak{R}}^{(n)}} L^2 \left(\cos \tilde{\theta}_{\mathfrak{S}}^{(n)} + \cos \tilde{\theta}_{\mathfrak{R}}^{(n)} \right) \text{sinc}(kL\mathcal{D}_{\tilde{x}}) \text{sinc}(kL\mathcal{D}_{\tilde{y}}) e^{-j(\varphi_{\mathfrak{S}} + \varphi_{\mathfrak{R}})} \quad (2)$$

where η is the free-space impedance, while $d_{\mathfrak{S}}^{(n)}$ and $d_{\mathfrak{R}}^{(n)}$ are the distances travelled by the incident wave from the BS to the barycenter of the n -th ($n = 1, \dots, N$) tile ($d_{\mathfrak{S}}^{(n)} = |\mathbf{r}_{BS} - \mathbf{r}_S^{(n)}|$) and by the reflected wave from the barycenter of the n -th ($n = 1, \dots, N$) tile to the point $\mathbf{r}_{\Omega}^{(n)}$

⁽¹⁾The following relationships between the reference and the local coordinate systems hold true: $\tilde{x} = y$, $\tilde{y} = z - z_S^{(n)}$, and $\tilde{z} = x$.

where the peak of the reflected beam, generated from the same n -th tile, is directed ($d_{\mathfrak{R}}^{(n)} = \left| \mathbf{r}_S^{(n)} - \mathbf{r}_\Omega^{(n)} \right|$), respectively. Moreover, $\varphi_{\mathfrak{S}}$ is the phase associated to the modulation of the signal generated by the *BS*, $\varphi_{\mathfrak{R}}$ is the phase term that can be engineered with the design of the surface, while $\mathcal{D}_{\tilde{x}} = \sin \tilde{\theta} \cos \tilde{\phi} - \sin \tilde{\theta}_{\mathfrak{R}}^{(n)} \cos \tilde{\phi}_{\mathfrak{R}}^{(n)}$ and $\mathcal{D}_{\tilde{y}} = \sin \tilde{\theta} \sin \tilde{\phi} - \sin \tilde{\theta}_{\mathfrak{R}}^{(n)} \sin \tilde{\phi}_{\mathfrak{R}}^{(n)}$.

To improve the coverage within the *AoI* by guaranteeing a suitable intensity of the signal from the *BS* by means of the reflection from the *EMS*, the following synthesis problem is formulated:

Modular Reflecting EM Skin (MREMS) Design Problem - Given an admissible skin surface \mathcal{S} discretized into N square tiles, $\{\mathcal{S}^{(n)}; n = 1, \dots, N\}$, and an *AoI* Ω , select the minimum number of tiles M (i.e., $M \leq N$), which reflect the *EM* wave from the *BS* towards the corresponding focusing points, $\{\mathbf{r}_\Omega^{(n)}; n = 1, \dots, M\}$, within the *AoI* ($\mathbf{r}_\Omega^{(n)} \in \Omega$), so that the power collected by a receiver at the position \mathbf{r}_u of the *AoI* ($\mathbf{r}_u \in \Omega$), $\mathcal{P}_{\mathfrak{R}}(\mathbf{r}_u)$ ($\mathcal{P}_{\mathfrak{R}}(\mathbf{r}) \triangleq \sum_{m=1}^M \left| E_{\mathfrak{R}}^{(m)}(\mathbf{r}) \right|^2$), fulfils the condition

$$\mathcal{P}_{\mathfrak{R}}(\mathbf{r}_u) \geq \mathcal{P}_{th} \quad (3)$$

where \mathcal{P}_{th} is a user-defined coverage threshold ($\mathcal{P}_{th} \geq \mathcal{P}_{bls}$, \mathcal{P}_{bls} being the minimum level for a wireless connection).

3 MREMS Synthesis Method

The *MREMS* Design Problem is addressed through a multi-objective optimization strategy based on a binary implementation of the *NSGA-II* [24]. Towards this end, the presence/absence of a tile on the final *EMS* layout \mathcal{S}_{opt} is mathematically modeled by means of a binary variable, t_n ($t_n \in \{0, 1\}$) ($n = 1, \dots, N$). If $t_n = 1$, then the n -th ($n = 1, \dots, N$) tile $\mathcal{S}^{(n)}$ is present on the facade of the building and it contributes to the reflection of the *EM* wave towards the *AoI*. Otherwise (i.e., $t_n = 0$), the n -th ($n = 1, \dots, N$) tile $\mathcal{S}^{(n)}$ is not installed on the external wall of the building, which maintains its original scattering properties without contributing to the enhancement of the signal in Ω . Accordingly, an admissible layout of the *EMS* (i.e., an arrangement of tiles over the available surface \mathcal{S}) is univocally described by the binary vector \mathbf{T} ($\mathbf{T} \triangleq \{t_n; n = 1, \dots, N\}$).

In order to determine the final structure of the *EMS*, \mathcal{S}_{opt} , namely the best subset of M tiles among the N admissible ones to be installed in \mathcal{S} , the problem is formulated as an optimization one by defining suitable optimization objectives aimed at quantifying the mismatch between the desired coverage (3) with that afforded by a trial *EMS* arrangement, \mathbf{T} , as well as the complexity of the final layout of the *EMS*, \mathbf{T}_{opt} . More specifically, the following two cost functions are defined. The former is the “*coverage term*”, $\Phi_1(\mathbf{T})$, given by

$$\Phi_1(\mathbf{T}) \triangleq \frac{1}{U} \sum_{u=1}^U \frac{\left| \sum_{n=1}^N t_n \mathcal{P}_{\mathfrak{R}}^{(n)}(\mathbf{r}_u; \mathbf{T}) - \mathcal{P}_{th} \right|}{\mathcal{P}_{th}} \mathcal{H} \left\{ \mathcal{P}_{th} - \sum_{n=1}^N t_n \mathcal{P}_{\mathfrak{R}}^{(n)}(\mathbf{r}_u; \mathbf{T}) \right\}, \quad (4)$$

while the latter is the “*complexity term*” defined as

$$\Phi_2(\mathbf{T}) \triangleq \frac{M}{N} \quad (5)$$

where U is the number of receivers, which are uniformly distributed inside the *AoI* Ω , and M ($M = \sum_{n=1}^N t_n$) is the number of tiles composing the *EMS*. Moreover, $\mathcal{H}(\cdot)$ is the Heaviside function equal to 1 when the argument is positive (i.e., $\mathcal{P}_{th} > \mathcal{P}_{\mathfrak{R}}(\mathbf{r}_u; \mathbf{T}) \rightarrow$ the power strength at \mathbf{r}_u is below the desired value) and 0 otherwise [i.e., $\mathcal{P}_{th} \leq \mathcal{P}_{\mathfrak{R}}(\mathbf{r}_u; \mathbf{T}) \rightarrow$ the coverage condition (3) is fulfilled].

Since the two cost functions to be minimized impose, on the one hand, the fitting of the coverage condition (4), while, on the other hand, the reduction of the number of tiles to minimize the area/cost of the skin (5), they are by definition conflicting. Indeed, a larger number of tiles leads to a stronger electric field in Ω and vice versa. Thus, the optimization problem turns out to be natively multi-objective and a natural solution strategy is that of defining a Pareto front of multiple optimal solutions, each being a valid trade-off to be considered for the final implementation of the *EMS* on the building facade. Such a multiplicity of solutions gives to the designer the possibility of choosing the *EMS* layout to be implemented according to its feeling and other non-functional constraints (e.g., architectural and landscaping restrictions, costs, etc ...). Following such a guideline, the binary *NSGA-II* [24] is chosen as optimization algorithm because of the binary nature of the design problem at hand (\mathbf{T} being a binary vector) and the need of synthesizing multiple trade-off solutions among the conflicting objectives. Moreover,

thanks to its hill-climbing features [28], the Genetic Algorithm (GA) has global optimization features, which are here compulsory due to the non-convex behaviors of the cost functions. Indeed, Φ_1 and Φ_2 are non-continuous functions also characterized by the presence of local minima (i.e., sub-optimal solutions of the corresponding *EMS* design problem).

More in detail, the following implementation of the binary *NSGA-II* is taken into account:

- **Step 0 - NSGA-II Setup.** Select the number of P individuals (i.e., trial layouts of the *EMS*) of the *GA* population and set the control parameters of the *NSGA-II*, namely the crossover rate, \wp_c , the polynomial mutation rate, \wp_m , the distribution index for both the crossover, \aleph_c , and the mutation rate, \aleph_m , and the maximum number of iterations, I , i being the iteration index ($i = 0, \dots, I$);
- **Step 1 - Population Initialization** ($i = 0$). Randomly set the initial trial solutions, $\{\mathbf{T}_i^{(p)}; p = 1, \dots, P\}$, and compute the cost function terms, $\Phi_{1,i}^{(p)} = \Phi_1(\mathbf{T}_i^{(p)})$ and $\Phi_{2,i}^{(p)} = \Phi_2(\mathbf{T}_i^{(p)})$, for each individual of the population ($p = 1, \dots, P$);
- **Step 2 - EMS Optimization** ($i = 1, \dots, I$). Apply the evolutionary operators of the *NSGA-II* to iteratively ($i \leftarrow i+1$) generate the offsprings, $\{\mathbf{T}_i^{(p)}; p = 1, \dots, P\}$, from the current population of parents, $\{\mathbf{T}_{i-1}^{(p)}; p = 1, \dots, P\}$, and compute their fitness values (4) and (5). Stop the iterative process when the maximum number of iterations ($i = I$) is reached;
- **Step 3 - Final Trade-Off EMS Design.** Select the set of O trial solutions that are non-dominated and belonging to the optimized Pareto front [24], $\{\mathbf{T}_{opt}^{(o)}; o = 1, \dots, O\}$. Such solutions are ordered according to the Φ_2 cost function value, namely $\mathbf{T}_{opt}^{(o)} \Big|_{o=1} = \min_{o=1, \dots, O} \left\{ \Phi_2(\mathbf{T}_{opt}^{(o)}) \right\}$ and $\mathbf{T}_{opt}^{(o)} \Big|_{o=O} = \max_{o=1, \dots, O} \left\{ \Phi_2(\mathbf{T}_{opt}^{(o)}) \right\}$. For a given o -th ($o = 1, \dots, O$) Pareto optimal solution, $\mathbf{T}_{opt}^{(o)}$, place the n -th ($n = 1, \dots, N$) tile $\mathcal{S}^{(n)}$ of the skin at the position $\mathbf{r}_S^{(n)}$ on the wall of the building if $t_{n,opt}^{(o)} = 1$.

4 Numerical Results

The objective of this section is twofold. On the one hand, the critical evaluation of the impact on the wireless coverage of using modular *EMS*s. On the other, the assessment of the effectiveness

of the proposed design method by considering different scenarios and tiles, while validating (2) through full-wave simulations with *ANSYS HFSS* [30].

As for this latter, the validation benchmark consists of a single ($N = 1$) tile located on the $y - z$ plane at the center of a Cartesian coordinate system and illuminated by a millimeter ($f = 27$ [GHz]) plane wave generated from the *BS* (1) that impinges with an orthogonal incidence $(\theta_{\mathfrak{S}}^{(1)}, \phi_{\mathfrak{S}}^{(1)}) = (0, 0)$ [deg] on the tile with a vertical polarized (i.e., $\hat{\mathbf{e}}_r = \hat{\mathbf{y}}$) electric field. The distance between the *BS* and the tile has been chosen equal to $d_{\mathfrak{S}}^{(1)} = 100$ [m] ($\rightarrow 9 \times 10^3 \lambda$), while the side and the square area of the tile has been set to $L^{(1)} = 25 \lambda$ and $\Delta \mathcal{S}^{(1)} \simeq 0.277 \times 0.277$ [m²], respectively.

The realistic *EMS* tile has been modeled with the *ANSYS HFSS* software as a metasurface defined by a lattice of unit cells uniformly-space along the x - and the y -axis by $\frac{\lambda}{2}$. Each unit-cell is composed by a square metallic patch printed on a single-layer Rogers 3003 dielectric substrate with thickness 5.08×10^{-4} [m] [Fig. 3(a)]. The single-tile *EMS* has been then designed by shaping the metallic patches of the metasurface so that it reflects the impinging wave towards the direction $(\theta_{\mathfrak{R}}^{(1)}, \phi_{\mathfrak{R}}^{(1)}) = (40, -20)$ [deg] [27].

For comparison purposes, the power, $\mathcal{P}_{\mathfrak{R}}(\mathbf{r})$, reflected from the realistic [Fig. 3(b)] and the ideal [Fig. 3(c)] tiles on a sphere at a distance of 5 [m] from the skin barycenter $\mathbf{r}_{\mathcal{S}}^{(0)}$ is shown in Fig. 3. As for the reflected electric field computed in *HFSS*, only the co-polar component is shown for the sake of comparison with the field reflected from ideal skin, which is not affected by the polarization loss [31]. Albeit the presence of undesired sidelobes, which are generally unavoidable when dealing with a real implementation of a low-cost artificial metasurface, the main lobes have a similar shape in both cases and they are steered towards the same desired angular direction [Figs. 3(b)-3(c)]. Since the pattern generated from the ideal tile according to (2) is free of undesired sidelobes and polarization losses, it seems reasonable to infer that the modular *EMS*s synthesized in this work will represent reference ideal solutions. From an operative viewpoint, this means that the number M of tiles composing the synthesized *EMS* layout has to be considered as a lower bound (i.e., the minimum number of tiles for approximating a project target) to be probably increased when going to the implementation of the *EMS* in a real scenario.

Moving to the design of modular reflecting *EMSs* for an enhanced wireless coverage, the first test case (*Simple Skin Layout - Orthogonal Incidence*) refers to the urban scenario depicted in Fig. 4(a) where the *BS* is located at \mathbf{r}_{BS} with Cartesian coordinates $(x_{BS}, y_{BS}, z_{BS}) = (100, 0, 10)$ [m]. The height of the *BS* from the ground (i.e., $z_{BS} = 10$ [m]) has been set according to the *3GPP* guidelines for the *Urban-Micro (UMi)* cell scenario [32]. Moreover, the *BS* has been assumed to radiate a plane wave at $f = 27$ [GHz] having the electric field vertically-polarized ($\hat{\mathbf{e}}_r = \hat{\mathbf{z}}$) with unitary amplitude $E_{\mathfrak{S}} = 1.0$ [V/m] that impinges from the ϕ -normal direction ($\phi_{\mathfrak{S}}^{(0)} = 0.0$ [deg]) on the *EMS* placed on the $y - z$ plane [i.e., $x_S^{(n)} = 0$ ($n = 1, \dots, N$)] [Fig. 4(b)] at a distance of $d_{\mathfrak{S}}^{(0)} = 100$ [m] from the *BS*. The admissible surface \mathcal{S} for the deployment of the artificial *EMS* on the building facade [Fig. 4(b)] has been chosen with an area $\Delta\mathcal{S} = 15$ [m²] and it extends within the range -2.5 [m] $\leq y_S \leq 2.5$ [m] and 5.0 [m] $\leq z_S \leq 8.0$ [m] along the y - and the z -axis, respectively. Such an area \mathcal{S} has been partitioned into $N = 60$ square sub-domains of size $\Delta\mathcal{S}^{(n)} = L^{(n)} \times L^{(n)}$ ($n = 1, \dots, N$) being $L^{(n)} = 0.5$ [m], so that there are $N_y = 10$ and $N_z = 6$ partitions along the y - and the z -axis, respectively (i.e., $N = N_y \times N_z$). By enumerating the admissible locations of the *EMS* tiles in a raster scan way, starting from the top left corner of \mathcal{S} , the barycenter of the n -th ($n = 1, \dots, N$) sub-domain of \mathcal{S} has the following coordinates

$$\begin{aligned} y_S^{(n)} &= y_S^{(1)} + \left(n - 1 - \left\lfloor \frac{n-1}{N_y} \right\rfloor N_y \right) \times L^{(n)} \\ z_S^{(n)} &= z_S^{(1)} - \left\lfloor \frac{n-1}{N_y} \right\rfloor \times L^{(n)} \end{aligned} \quad (6)$$

($n = 2, \dots, N$), $y_S^{(1)} = -2.25$ [m] and $z_S^{(1)} = 7.75$ [m] being the coordinates of the barycenter of the first ($n = 1$) location admissible for a tile.

The goal of the *EMS* design is that of enhancing the power strength in the *AoI* Ω of size $\Delta\Omega = 10 \times 50$ [m²] located in $x_{\Omega}^{(0)} = 80.35$ [m] and $y_{\Omega}^{(0)} = 95.75$ [m] [Fig. 4(a)] along the azimuth direction $\phi_{\mathfrak{R}}^{(0)} = 50.0$ [deg] with respect to the *EMS*, $\mathcal{P}_{th} = -70$ [dB] being the threshold on the desired coverage in (4), while the “no connection” power level has been set to $\mathcal{P}_{bts} \approx -100$ [dB]. In order to assess the “coverage” condition within the *AoI*, $U = 500$ ideal receivers have been uniformly-distributed within Ω , that is one receiver every $\Delta\Omega = 1$ [m²], at the height

$z_u = 1.5$ [m] to emulate users on the ground [32].

Concerning the *NSGA-II* algorithm, the following setup of the control parameters has been used: $P = 2 \times N$, $I = 1000$, $\wp_c = 1.0$, $\wp_m = \frac{1}{N}$, $\aleph_c = 15$, and $\aleph_m = 20$. Moreover, each simulation has been repeated 50 times with different random seeds to statistically validate the results from the stochastic optimization. However, since all simulations led to similar Pareto fronts at convergence ($i = I$), only the solutions of a representative run will be reported and discussed in the following.

Figure 5 shows the population of trial solutions, $\{\mathbf{T}_i^{(p)}; p = 1, \dots, P\}$, at the iterations $i = 100$, $i = 500$, and $i = I$ in the space of the objectives along with the Pareto front of $O = 12$ non-dominated solutions at the convergence ($i = I$), $\{\mathbf{T}_{opt}^{(o)}; o = 1, \dots, O\}$. Let us now analyze the *EMS* solution that fully fits the coverage requirements [i.e., $\Phi_1(\mathbf{T}_{opt}^{(o)}) = 0$], which corresponds to the O -th representative point of the Pareto front, whose chromosome has $M = 12$ bits at one (i.e., $t_{n,opt}^{(o)} \Big|_{o=12} = 1$, $n = \{3, 4, 5, 6, 8, 12, 30, 32, 43, 44, 45, 46\}$) so that the *EMS* layout turns out being composed by $M = 12$ tiles as shown in Fig. 6(a). The support of such an *EMS* amounts to $\Delta\mathcal{S}_{opt}^{(o)} \Big|_{o=12} = 3$ [m²], which is one fifth of the whole admissible *EMS* surface (i.e., $\frac{\Delta\mathcal{S}_{opt}^{(o)} \Big|_{o=12}}{\Delta\mathcal{S}} = 20$ %). The coverage improvement enabled by the installation of such an artificial skin on the building facade is pointed out in Fig. 6(b) where the map of the reflected power $\mathcal{P}_{\Re}(\mathbf{r})$ at $z = 1.5$ [m] from the ground is shown in a region Ψ , around the *AoI*, of extension $\Delta\Psi = 200 \times 200$ [m²]. As it can be observed, the power intensity along the direction of the street passing through Ω has been significantly increased. As a matter of fact, the signal turns out to be stronger not only in Ω , but also before and after [Fig. 6(b)] since the skin tiles generate simple pencil beams (2) with an elongated footprint on the ground, the dots in Figs. 6(b)-6(c) being the $M = 12$ points $\mathbf{r}_{\Omega}^{(n)}$, $n = \{3, 4, 5, 6, 8, 12, 30, 32, 43, 44, 45, 46\}$ where the peaks of the beams reflected from the M *EMS* tiles are directed. Regardless of the simplicity of the beam afforded by a single *EMS* tile, the combined use of multiple/modular tiles has allowed to reach the desired average power threshold $\mathcal{P}_{th} = -70$ [dB] (i.e., $\Phi_1(\mathbf{T}_{opt}^{(o)} \Big|_{o=12}) = 0$) in the whole *AoI* as shown in Fig. 6(c), $\gamma - \xi$ being the Ω local coordinate system [see Fig. 6(b)]. Indeed, the statistics of the power reflected in Ω are: $\min_{\mathbf{r} \in \Omega} \left\{ \mathcal{P}_{\Re}(\mathbf{r}_u; \mathbf{T}_{opt}^{(o)} \Big|_{o=12}) \right\} = -69.9$ [dB], $\max_{\mathbf{r} \in \Omega} \left\{ \mathcal{P}_{\Re}(\mathbf{r}_u; \mathbf{T}_{opt}^{(o)} \Big|_{o=12}) \right\} = -63.0$ [dB], and $\text{avg}_{\mathbf{r} \in \Omega} \left\{ \mathcal{P}_{\Re}(\mathbf{r}_u; \mathbf{T}_{opt}^{(o)} \Big|_{o=12}) \right\} = -66.8$

[dB], respectively (Tab. I).

For the sake of completeness, other two representative solutions of the Pareto front in Fig. 5 are analyzed. The *EMS* layouts and the maps of the power reflected in Ψ of the solution with minimum complexity ($o = 1$ - Fig. 5) and the one having $\Phi_1 \left(\mathbf{T}_{opt}^{(o)} \right) \Big|_{o=4} \approx 0.1$ (i.e., $\text{avg}_{\mathbf{r} \in \Omega} \left\{ \mathcal{P}_{\mathcal{R}} \left(\mathbf{r}_u; \mathbf{T}_{opt}^{(o)} \Big|_{o=12} \right) \right\} = -77$ [dB]) are reported in Fig. 7.

The minimum complexity *EMS* (i.e., $\Phi_2 \left(\mathbf{T}_{opt}^{(o)} \Big|_{o=1} \right) = \frac{1}{60}$) needs only one ($M = 1$) tile [Fig. 7(a)], but the average power level in Ω reduces of $\delta\Phi_1 \Big|_{o=1}^{o=12} = 17.9$ [dB] ($\delta\Phi \Big|_{o'}^o \triangleq \Phi \left(\mathbf{T}_{opt}^{(o)} \right) - \Phi \left(\mathbf{T}_{opt}^{(o')} \right)$; $o, o' \in [1, O]$) with respect to that in Fig. 6(a). Owing to the presence of a single tile, the map of the *EM* power in Fig. 7(c) shows the classical footprint of a pencil beam characterized by a mainlobe focused in the point $\mathbf{r}_{\Omega}^{(n)} \Big|_{n=28}$ within Ω [Fig. 7(c)] along the central line of the *AoI* ($\xi = 0$) [Fig. 7(e)], while there are portions of Ω close to $\xi = \pm 5$ [m] where the power strength is very low [Fig. 7(e)]. Quantitatively, it turns out that the condition $\mathcal{P}_{th} \leq \mathcal{P}_{\mathcal{R}} \left(\mathbf{r}_u; \mathbf{T}_{opt}^{(o)} \Big|_{o=1} \right)$ never holds true [Fig. 7(e)] since also the power peak is below the desired *QoS* threshold ($\mathcal{P}_{\mathcal{R}} \left(\mathbf{r}_u; \mathbf{T}_{opt}^{(o)} \Big|_{o=1} \right) = -78.1$ [dB]). Moreover, the minimum level of the power reflected within the *AoI* by such a single-tile *EMS* of side $L^{(1)} = 0.5$ [m] is equal to $\min_{\mathbf{r} \in \Omega} \left\{ \mathcal{P}_{\mathcal{R}} \left(\mathbf{r}_u; \mathbf{T}_{opt}^{(o)} \Big|_{o=1} \right) \right\} = -173.9$ [dB] (Tab. I), that is (well) below the “connectivity” threshold of $\mathcal{P}_{bls} = -100$ [dB]. Such an undesired condition verifies in other portions of Ω where there is not enough signal for assuring the users’ connections [$\mathcal{P}_{\mathcal{R}} \left(\mathbf{r}_u; \mathbf{T}_{opt}^{(o)} \Big|_{o=1} \right) < \mathcal{P}_{bls}$ - Fig. 7(g)].

By using three more tiles [i.e., $M = 4$ - Fig. 7(b)], the power level reflected on Ω turns out significantly higher [Fig. 7(d)], the average power being increased of almost ten times (i.e. $\delta\Phi_1 \Big|_{o=1}^{o=4} = 9.7$ [dB]), and there are no more “no connection” zones within Ω [Fig. 7(h)] since $\min_{\mathbf{r} \in \Omega} \left\{ \mathcal{P}_{\mathcal{R}} \left(\mathbf{r}_u; \mathbf{T}_{opt}^{(o)} \Big|_{o=4} \right) \right\} = -90.9$ [dB] (Tab. I), even though the power peak is still slightly lower than the *QoS* threshold ($\max_{\mathbf{r} \in \Omega} \left\{ \mathcal{P}_{\mathcal{R}} \left(\mathbf{r}_u; \mathbf{T}_{opt}^{(o)} \Big|_{o=4} \right) \right\} = -71.7$ [dB]).

In the second test case (*Simple Skin Layout - Oblique Incidence*), the field generated from the *BS* has been assumed impinging on the *EMS* with an oblique incidence on the azimuth plane (i.e., $\phi_{\mathcal{S}}^{(0)} = 20$ [deg]), being $(x_{BS}, y_{BS}, z_{BS}) = (93.9, 34.2, 10)$ [m] such that $d_{\mathcal{S}}^{(0)} = 100$ [m] as in the previous example [Fig. 8(a)]. All other features concerned with the *EM* field generated from the *BS* (i.e., frequency and polarization), the area and the discretization of \mathcal{S} ,

and the coverage area under analysis Ω have been kept unaltered from the first test case.

The Pareto front of the O optimal trade-off solutions determined by the proposed *NSGA-II* based approach is compared in Fig. 8(b) with that obtained in the “normal incidence” case (Fig. 5). The reader can observe that the Pareto front of the “oblique incidence” scenario consists of $O = 14$ *EMS* designs (vs. $O = 12$ - “normal incidence”) and it turns out that the oblique incidence from the *BS* needs a higher number of tiles to yield the same coverage of the “normal incidence” solutions [Fig. 8(b)]. As expected, a wider area is now required because of the reduction of the effective area of the *EMS* (2) since a lower amount of power is intercepted from the incident wave with the same area of the “normal incidence” *EMS*.

Figure 9 summarizes the characteristics of the O -th ($O = 14$) solution that fits the coverage requirement [i.e., $\mathcal{P}_{\mathbb{R}}(\mathbf{r}_u; \mathbf{T}_{opt}^{(O)}) \geq \mathcal{P}_{th} \rightarrow \Phi_1(\mathbf{T}_{opt}^{(O)}) = 0$]. More in detail, the layout of the corresponding *EMS* is composed by $M = 14$ tiles [Fig. 9(a)], that is two more than those of the O -th *EMS* for the normal incidence, and the arising tiles arrangement is also quite different [Fig. 9(a) vs. Fig. 6(a)]. On the contrary, the power distributions are quite similar as pictorially shown by comparison of the maps in Figs. 9(b)-9(c) with those in Figs. 6(b)-6(c) and also confirmed by the statistics of the power reflected by the *EMS* within the *AoI* (Tab. I).

Indeed, the differences among the values of the statistical indices are null or negligible (i.e.,

$$\delta \mathcal{P}_{\mathbb{R}}^{min}]_{Normal}^{Oblique} = 0.0 \text{ [dB]}, \delta \mathcal{P}_{\mathbb{R}}^{max}]_{Normal}^{Oblique} = 0.2 \text{ [dB]}, \text{ and } \delta \mathcal{P}_{\mathbb{R}}^{av}]_{Normal}^{Oblique} = \delta \Phi_1]_{Normal}^{Oblique} = -0.1 \text{ [dB]}, \text{ being } \delta \mathcal{P}_{\mathbb{R}}^{stat}]_{Normal}^{Oblique} \triangleq \text{stat}_{\mathbf{r} \in \Omega} \left\{ \mathcal{P}_{\mathbb{R}} \left(\mathbf{r}_u; \mathbf{T}_{opt}^{(o)} \right) \Big|_{o=O}^{Oblique} \right\} - \text{stat}_{\mathbf{r} \in \Omega} \left\{ \mathcal{P}_{\mathbb{R}} \left(\mathbf{r}_u; \mathbf{T}_{opt}^{(o)} \right) \Big|_{o=O}^{Normal} \right\}$$

- Tab. I).

The third design experiment (*Simple Skin Layout - Varying Tiles Size*) is concerned with a surface \mathcal{S} still discretized with uniform tiles, but considering different tile sizes: $L^{(n)} = 1.0$ [m] [$\rightarrow N = N_y \times N_z = 5 \times 3 = 15$ - Fig. 10(a)] or $L^{(n)} = 0.25$ [m] [$\rightarrow N = N_y \times N_z = 20 \times 12 = 240$ - Fig. 10(b)] ($n = 1, \dots, N$). In the former case, there are few admissible tiles reflecting a narrow beam towards the *AoI*, while the number of tiles and *DoFs* is 16 times larger in the latter case where the beam reflected by each m -th ($m = 1, \dots, M$) installed tile has a broader coverage.

The *NSGA-II* optimization has been run for both tile sizes and the Pareto fronts obtained at the convergence ($i = I$) are shown in Fig. 11(a) along with that of Fig. 5, which is related to the

tile size $L^{(n)} = 0.5$ [m] ($n = 1, \dots, N$). The plots in Fig. 11(a) indicate that, the wider the tile size, the higher is the value of the complexity index Φ_2 to fulfil (3). Furthermore, it is worth highlighting that when $L^{(n)} = 1.0$ [m], no solution of the Pareto front satisfies the coverage requirement since $\Phi_1 \left(\mathbf{T}_{opt}^{(O)} \right) > 0$, while the coverage condition holds true using smaller tiles. The same conclusions arise when extending the coverage area Ω from $\Delta\Omega = 10 \times 50$ [m²] [Fig. 11(a)] up to $\Delta\Omega = 10 \times 100$ [m²] [Fig. 11(b)]. For this latter case, the layouts and the coverage maps of the solutions providing the best coverage (i.e., the O -th of the Pareto front) for each tile size are shown in Fig. 12. By analyzing the power distributions in Figs. 12(d)-12(f), it turns out that the main advantage of using larger tiles, which reflect narrower beams, is the capability of better focusing the reflected field only along the direction of the *AoI* [Fig. 12(f) vs. Fig. 12(d)]. This is not for free and the cost to pay is that of having a very large *EMS* composed by $M = 13$ tiles, each of $\Delta\mathcal{S}^{(m)} = 1$ [m²] ($m = 1, \dots, M$), for a total surface of $\Delta\mathcal{S}_{opt}^{(O)} \Big|_{L=1.0 \text{ [m]}} = 13$ [m²], while the area occupied by the *EMS* when using square tiles of size $L^{(n)} = 0.25$ [m] [Fig. 12(a)] and $L^{(n)} = 0.5$ [m] [Fig. 12(b)] amounts to $\Delta\mathcal{S}_{opt}^{(O)} \Big|_{L=0.25 \text{ [m]}} \simeq 1.69$ [m²] and $\Delta\mathcal{S}_{opt}^{(O)} \Big|_{L=0.5 \text{ [m]}} = 5$ [m²], respectively. This means that the limited focusing capability of smaller tiles is balanced by a reduction of the required *EMS* extension, thus a lower cost of the *EMS*.

In the last design example (*Complex Skin Layout - Orthogonal Incidence*), the admissible region \mathcal{S} on the building facade is more complex [Fig. 13(a)] since the area dedicated to the *EMS* deployment is smaller and there are more architectural constraints (e.g., misaligned windows and open window shutters) as in historical buildings. As for the descriptive parameters of the scenario at hand, they have been defined as in the “*Simple Skin Layout - Orthogonal Incidence*” case, but a larger *AoI* (i.e., $\Delta\Omega = 10 \times 100$ [m²]) has been considered.

The evolution ($i = 100$, $i = 500$, and $i = I$) of the population of *EMS* trial solutions, $\left\{ \mathbf{T}_i^{(p)}; p = 1, \dots, P \right\}$, in the space of the objectives is shown in Fig. 13(b) together with the Pareto front at convergence ($i = I$), which includes $O = 31$ non-dominated solutions, $\left\{ \mathbf{T}_{opt}^{(o)}; o = 1, \dots, O \right\}$. As it can be noticed [Fig. 13(b)], 15 *EMS* of the Pareto front have values of the coverage index smaller than $\Phi_1 \left(\mathbf{T}_{opt}^{(o)} \Big|_o \right) < 10^{-2}$.

The O -th solution, which fully satisfies the coverage requirements, is done by $M = 32$ tiles of

size $\Delta\mathcal{S}^{(m)} = 0.5 \times 0.5 \text{ [m}^2\text{]}$ ($m = 1, \dots, M$) and it covers a surface area of $\Delta\mathcal{S}_{opt}^{(O)} = 8 \text{ [m}^2\text{]}$ [Fig. 14(a)]. Despite the irregularity of the *EMS* layout, the coverage maps in Figs. 14(b)-14(d) confirm that the proposed *EMS* design method properly selects, from the admissible pool, a subset of tiles that guarantees the required power level within the *AoI* Ω (Tab. I).

5 Conclusions

Within the *SEME* vision, this paper has proposed a novel strategy to improve the signal strength in urban areas where the power radiated by the *BS* is too strongly attenuated. More specifically, such an approach proposes the use of modular, passive, and static artificial metasurfaces to be installed/embedded on the facades of urban buildings, such as coating skins, to enhance the coverage by reflecting the *EM* wave coming from the *BS* towards the desired directions within an *AoI*. In order to fulfil user-defined coverage conditions, while minimizing the cost/complexity, the design of the *EMS* has been cast as a multi-objective optimization problem and it has been addressed by means of a binary implementation of the *NSGA-II* algorithm.

From a technological and methodological viewpoint, the main novelties, to the best of the authors' knowledge, of this research work can be summarized as follows:

- the introduction for the first time of a novel cost-effective solution, to be possibly implemented through cheap printed technology, for the large scale deployment of artificial metasurfaces to be installed on the facades of buildings for improving the wireless coverage in urban scenarios;
- the suitability of the proposed technological solution in future wireless networks thanks to its “green” (i.e., passive) and non-invasive (i.e., low profile and without heavy architectural impact) nature;
- the development of a customized design strategy to enable an effective/efficient optimization-based design of (also large) *EMS*s composed by simple (also non-homogeneous) tiles.

From the numerical assessment, which has been carried out by considering realistic topological urban scenarios and a millimeter-wave 5G frequency band, the following outcomes can be

drawn:

- the use of tiled *EMS*s always improves the coverage of the *AoI*;
- the (*NSGA-II*)-based synthesis approach provides the designer with a Pareto front of multiple *EMS* solutions, which are trade-offs between coverage requirements and complexity of the *EMS* layout. In all the considered scenarios, an *EMS* that fulfils the user-defined coverage condition (i.e., not only the user connection) has been (generally) found without using the whole area available on the facade of the building;
- the number and the positions of the tiles of the *EMS* layout depend on the relative position between the *BS* and the *AoI*. Moreover, the dimension (e.g., small, medium, large) and the distribution (e.g., uniform or non-uniform) of the tiles composing the *EMS* are other *DoFs*, which can be exploited to fit the coverage conditions as well as other architectural constraints (e.g., misaligned windows and open window shutters).

Future research activities, beyond the scope of this paper, will integrate the design of the tiles layout within the proposed iterative optimization loop in order to take into account non-ideal reflections and polarization losses. Moreover, the presence of multiple *BS*s and *AoI*s will be dealt with towards the definition of a tool for network planning.

Acknowledgements

This work benefited from the networking activities carried out within the Project “CYBER-PHYSICAL ELECTROMAGNETIC VISION: Context-Aware Electromagnetic Sensing and Smart Reaction (EMvisioning)” (Grant no. 2017HZJXSZ)“ funded by the Italian Ministry of Education, University, and Research under the PRIN2017 Program (CUP: E64I19002530001). Moreover, it benefited from the networking activities carried out within the Project “SPEED” (Grant No. 61721001) funded by National Science Foundation of China under the Chang-Jiang Visiting Professorship Program, the Project ‘Inversion Design Method of Structural Factors of Conformal Load-bearing Antenna Structure based on Desired EM Performance Interval’ (Grant no. 2017HZJXSZ) funded by the National Natural Science Foundation of China, and the Project

'Research on Uncertainty Factors and Propagation Mechanism of Conformal Load-bearing Antenna Structure' (Grant No. 2021JZD-003) funded by the Department of Science and Technology of Shaanxi Province within the Program Natural Science Basic Research Plan in Shaanxi Province. A. Massa wishes to thank E. Vico for her never-ending inspiration, support, guidance, and help.

References

- [1] R. L. Haupt, *Wireless Communications Systems: An Introduction*. Hoboken, NJ, USA: John Wiley & Sons, IEEE Press, 2020.
- [2] J. Korhonen, *Introduction to 4G Mobile Communications*. Boston, MA, USA: Artech House, 2014.
- [3] C. Cox, *An Introduction to 5G: The New Radio, 5G Network and Beyond*. Hoboken, NJ, USA: John Wiley & Sons, 2021.
- [4] K. Yu, L. Lin, M. Alazab, L. Tan, and B. Gu, “Deep learning-based traffic safety solution for a mixture of autonomous and manual vehicles in a 5G-enabled intelligent transportation system,” *IEEE Trans. Intell. Transp. Syst.*, vol. 22, no. 7, pp. 4337-4347, Jul. 2021.
- [5] C. Li, K. Hosseini, S. B. Lee, J. Jiang, W. Chen, G. Horn, T. Ji, J. E. Smee, and J. Li, “5G-based systems design for tactile internet,” *Proc IEEE*, vol. 107, no. 2, pp. 307-324, Feb. 2019.
- [6] A. Acemoglu, J. Kriegelstein, D. G. Caldwell, F. Mora, L. Guastini, M. Trimarchi, A. Vinciguerra, A. L. C. Carobbio, J. Hysenbelli, M. Delsanto, O. Barboni, S. Baggioni, G. Peretti, and L. S. Mattos, “5G robotic telesurgery: remote transoral laser microsurgeries on a cadaver,” *IEEE Trans. Med. Robot. Bionics*, vol. 2, no. 4, pp. 511-518, Nov. 2020.
- [7] M. Bennis, M. Debbah, and H. V. Poor, “Ultrareliable and low-latency wireless communication: tail, risk, and scale,” *Proc. IEEE*, vol. 106, no. 10, pp. 1834-1853, Oct. 2018.
- [8] M. Wang, F. Gao, S. Jin, and H. Lin, “An overview of enhanced massive MIMO with array signal processing techniques,” *IEEE J. Sel. Topics Signal Process.*, vol. 13, no. 5, pp. 886-901, Sep. 2019.
- [9] A. Puglielli, A. Townley, G. LaCaille, V. Milovanović, P. Lu, K. Trotskovsky, A. Whitcombe, N. Narevsky, G. Wright, T. Courtade, E. Alon, B. Nikolić, and A. M. Niknejad, “Design of energy- and cost-efficient massive MIMO arrays,” *Proc. IEEE*, vol. 104, no. 3, pp. 586-606, Mar. 2016.

- [10] W. Hong, Z. H. Jiang, C. Yu, D. Hou, H. Wang, C. Guo, Y. Hu, L. Kuai, Y. Yu, Z. Jiang, Z. Chen, J. Chen, Z. Yu, J. Zhai, N. Zhang, L. Tian, F. Wu, G. Yang, Z.-C. Hao, and J. Y. Zhou, "The role of millimeter-wave technologies in 5G/6G wireless communications," *IEEE J. Microw.*, vol. 1, no. 1, pp. 101-122, Jan. 2021.
- [11] "Special Issue on Smart Electromagnetic Environment," *IEEE Trans. Antennas Propag.*, vol. 69, no. 3, pp. 1838-1838, Mar. 2021.
- [12] M. Salucci, B. Li, A. Benoni, P. Rocca, and A. Massa, "Smart EM environment as enabling technology for future wireless systems," *14th Int. Congr. Artificial Mater. Novel Wave Phenomena* (Metamaterials 2020), 2020, New York, NY, USA, 28 Sep.-3 Oct. 2020, pp. 48-50.
- [13] F. Yang and Y. Rahmat-Samii, *Surface Electromagnetics with Applications in Antenna, Microwave, and Optical Engineering*, Cambridge, UK: Cambridge University Press, 2019.
- [14] M. Di Renzo, M. Debbah, D.-T. Phan-Huy, A. Zappone, M.-S. Alouini, C. Yuen, V. Sciancalepore, G.C. Alexandropoulos, J. Hoydis, H. Gacanin, J. de Rosny, A. Bounceur, G. Lerosey, and M. Fink, "Smart radio environments empowered by reconfigurable AI metasurfaces: An idea whose time has come," *EURASIP J. Wireless Commun. Netw.*, vol. 2019, no. 129, pp. 1-20, 2019.
- [15] E. Basar, M. Di Renzo, J. De Rosny, M. Debbah, M.-S. Alouini, and R. Zhang, "Wireless communications through reconfigurable intelligent surfaces," *IEEE Access*, vol. 7, pp. 116753-116773, 2019.
- [16] M. Di Renzo, A. Zappone, M. Debbah, M.-S. Alouini, C. Yuen, J. de Rosny, and S. Tretyakov, "Smart radio environments empowered by reconfigurable intelligent surfaces: How it works, state of research, and the road ahead," *IEEE J. Sel. Areas Commun.*, vol. 38, no. 11, pp. 2450-2525, Nov. 2020.

- [17] J. A. Hodge, K. V. Mishra, and A. I. Zaghloul, "Intelligent time-varying metasurface transceiver for index modulation in 6G wireless networks," *IEEE Antennas Wireless Propag. Lett.*, vol. 19, no. 11, pp. 1891-1895, Nov. 2020.
- [18] B. G. Kashyap, P. C. Theofanopoulos, Y. Cui, and G. C. Trichopoulos, "Mitigating quantization lobes in mmWave low-bit reconfigurable reflective surfaces," *IEEE Open J. Antennas Propag.*, vol. 1, pp. 604-614, 2020.
- [19] A. Pitilakis, O. Tsilipakos, F. Liu, K. M. Kossifos, A. C. Tasolamprou, D.-H. Kwon, M. S. Mirmoosa, D. Manassis, N. V. Kantartzis, C. Liaskos, M. A. Antoniadis, J. Georgiou, C. M. Soukoulis, M. Kafesaki, and S. A. Tretyakov, "A multi-functional reconfigurable metasurface: electromagnetic design accounting for fabrication aspects," *IEEE Trans. Antennas Propag.*, vol. 69, no. 3, pp. 1440-1454, Mar. 2021.
- [20] Q. Wu, S. Zhang, B. Zheng, C. You, and R. Zhang, "Intelligent reflecting surface-aided wireless communications: A tutorial," *IEEE Trans. Commun.*, vol. 69, no. 5, pp. 3313-3351, May 2021.
- [21] M. Wang, S. Xu, F. Yang, and M. Li, "A 1-bit bidirectional reconfigurable transmit-reflect-array using a single-layer slot element with PIN diodes," *IEEE Trans. Antennas Propag.*, vol. 67, no. 9, pp. 6205-6210, Sep. 2019.
- [22] A. Massa, A. Benoni, P. Da R , S. K. Goudos, B. Li, G. Oliveri, A. Polo, P. Rocca, and M. Salucci, "Designing smart electromagnetic environments for next generation wireless communications," *Telecom*, Invited Feature Paper, vol. 2, no. 2, pp. 213-221, 2021.
- [23] J. Zhou, L. Kang, B. Tang, B. Tang, J. Huang, and C. Wang, "Adaptive compensation of flexible skin antenna with embedded fiber bragg grating," *IEEE Trans. Antennas Propag.*, vol. 67, no. 7, pp. 4385-4396, Jul. 2019.
- [24] K. Deb, A. Pratap, S. Agarwal, and T. Meyarivan, "A fast and elitist multiobjective Genetic Algorithm: NSGA-II," *IEEE Trans. Evol. Comput.*, vol. 6, no. 2, pp. 182-197, Apr. 2002.
- [25] A. Osipov and S. Tretyakov, *Modern Electromagnetic Scattering Theory with Applications*. Chichester, UK: John Wiley & Sons, 2017.

- [26] I. V. Lindell and A. Sihvola, *Boundary Conditions in Electromagnetics*. Hoboken, NJ, USA: John Wiley & Sons, IEEE Press, 2019.
- [27] G. Oliveri, A. Gelmini, A. Polo, N. Anselmi, and A. Massa, “System-by-design multi-scale synthesis of task-oriented reflectarrays,” *IEEE Trans. Antennas Propag.*, vol. 68, no. 4, pp. 2867-2882, Apr. 2020.
- [28] P. Rocca, M. Benedetti, M. Donelli, D. Franceschini, and A. Massa, “Evolutionary optimization as applied to inverse scattering problems,” *Inverse Prob.*, vol. 24, pp. 1-41, 2009.
- [29] F. H. Danufane, M. D. Renzo, J. de Rosny, and S. Tretyakov, “On the path-loss of reconfigurable intelligent surfaces: An approach based on Green’s theorem applied to vector fields,” *IEEE Trans. Commun.*, vol. 69, no. 8, pp. 5573-5592, Aug. 2021.
- [30] ANSYS Electromagnetics Suite - HFSS (2019). ANSYS, Inc.
- [31] C. A. Balanis, *Antenna Theory: Analysis and Design*. Hoboken, NJ, USA: John Wiley & Sons, 2005.
- [32] 3GPP, “Technical Specification Group Radio Access Network - Study on 3D channel model for LTE,” Technical Report, TR 36.873, v. 12.2.0, 2015-06.

FIGURE CAPTIONS

- **Figure 1.** *Problem geometry.* Illustrative sketches of the wireless communication scenario: (a) top view and (b) detailed zoom.
- **Figure 2.** *Problem geometry.* Graphical representation of the *EMS* local coordinate system.
- **Figure 3.** *Numerical Validation.* Layout of (a) the *ANSYS HFSS* model of the single-tile *EMS* and plot of (b)(c) the angular distribution of the power, $\mathcal{P}_{\mathfrak{R}}(\mathbf{r})$, reflected from the *EMS* on a sphere at a distance of 5 [m] and computed with (b) *ANSYS HFSS* or using (c) the closed-form relationship (2).
- **Figure 4.** *Numerical Validation - Simple Skin Layout - Orthogonal Incidence* ($f = 27$ [GHz], $\mathcal{S} = 15$ [m²], $L = 0.5$ [m], $N = 60$, $\Delta\Omega = 500$ [m²], $\mathcal{P}_{th} = -70$ [dB]). Sketch of (a) the scenario and of (b) the admissible surface \mathcal{S} along with its tile discretization.
- **Figure 5.** *Numerical Validation - Simple Skin Layout - Orthogonal Incidence* ($f = 27$ [GHz], $\mathcal{S} = 15$ [m²], $L = 0.5$ [m], $N = 60$, $\Delta\Omega = 500$ [m²], $\mathcal{P}_{th} = -70$ [dB]). Iterative ($i = 100$, $i = 500$, and $i = I$) evolution of the population of the P ($P = 2 \times N$) trial solutions, $\{\mathbf{T}_i^{(p)}; p = 1, \dots, P\}$, in the space of the design objectives and Pareto front at convergence ($i = I$), $\{\mathbf{T}_{opt}^{(o)}; o = 1, \dots, O\}$.
- **Figure 6.** *Numerical Validation - Simple Skin Layout - Orthogonal Incidence* ($f = 27$ [GHz], $\mathcal{S} = 15$ [m²], $L = 0.5$ [m], $N = 60$, $\Delta\Omega = 500$ [m²], $\mathcal{P}_{th} = -70$ [dB]). Plot of (a) the *EMS* layout of the O -th ($O = 12$) solution, $\mathcal{S}_{opt}^{(O)}$, of the Pareto front in Fig. 5 and map of the spatial distribution of the power, $\mathcal{P}_{\mathfrak{R}}(\mathbf{r})$, reflected from the *EMS* in (b) the region Ψ and within (c) the AoI Ω ($\Omega \subset \Psi$).
- **Figure 7.** *Numerical Validation - Simple Skin Layout - Orthogonal Incidence* ($f = 27$ [GHz], $\mathcal{S} = 15$ [m²], $L = 0.5$ [m], $N = 60$, $\Delta\Omega = 500$ [m²], $\mathcal{P}_{th} = -70$ [dB], $\mathcal{P}_{bls} \approx -100$ [dB]). Plot of (a)(b) the *EMS* layout and of (c)-(f) the corresponding spatial distributions of the power, $\mathcal{P}_{\mathfrak{R}}(\mathbf{r})$, reflected from the *EMS* along with (g)(h) the cover-

age/connectivity maps for (a)(c)(e)(g) the $o = 1$ and (b)(d)(f)(h) the $o = 4$ solutions of the Pareto front in Fig. 5.

- **Figure 8.** *Numerical Validation - Simple Skin Layout - Oblique Incidence* ($f = 27$ [GHz], $\mathcal{S} = 15$ [m²], $L = 0.5$ [m], $N = 60$, $\Delta\Omega = 500$ [m²], $\mathcal{P}_{th} = -70$ [dB]). Sketch of (a) the scenario and plot of (b) the Pareto front at convergence ($i = I$), $\{\mathbf{T}_{opt}^{(o)}; o = 1, \dots, O\}$.
- **Figure 9.** *Numerical Validation - Simple Skin Layout - Oblique Incidence* ($f = 27$ [GHz], $\mathcal{S} = 15$ [m²], $L = 0.5$ [m], $N = 60$, $\Delta\Omega = 500$ [m²], $\mathcal{P}_{th} = -70$ [dB]). Plot of (a) the EMS layout of the O -th ($O = 14$) solution, $\mathcal{S}_{opt}^{(O)}$, of the Pareto front in Fig. 5 and map of the spatial distribution of the power, $\mathcal{P}_{\mathfrak{R}}(\mathbf{r})$, reflected from the EMS in (b) the region Ψ and within (c) the AoI Ω ($\Omega \subset \Psi$).
- **Figure 10.** *Numerical Validation - Simple Skin Layout - Varying Tiles Size* ($f = 27$ [GHz], $\mathcal{S} = 15$ [m²], $N = \{240, 15\}$, $\mathcal{P}_{th} = -70$ [dB]). Sketches of the scenario and of the admissible surface \mathcal{S} along with its discretization when using tiles with side-length (a) $L = 1.0$ [m] and (b) $L = 0.25$ [m].
- **Figure 11.** *Numerical Validation - Simple Skin Layout - Varying Tiles Size* ($f = 27$ [GHz], $\mathcal{S} = 15$ [m²], $\mathcal{P}_{th} = -70$ [dB]). Plot of the Pareto fronts at convergence ($i = I$), $\{\mathbf{T}_{opt}^{(o)}; o = 1, \dots, O\}$, for different square tile sizes (L being the side-length of the tile) in correspondence with an AoI Ω of dimension (a) $\Delta\Omega = 10 \times 50 = 500$ [m²] and (b) $\Delta\Omega = 10 \times 100 = 1000$ [m²].
- **Figure 12.** *Numerical Validation - Simple Skin Layout - Varying Tiles Size* ($f = 27$ [GHz], $\mathcal{S} = 15$ [m²], $L = \{0.25, 0.5, 1.0\}$ [m], $N = \{240, 60, 15\}$, $\Delta\Omega = 1000$ [m²], $\mathcal{P}_{th} = -70$ [dB]). Plot of (a)-(c) the EMS layouts of the O -th solution, $\mathcal{S}_{opt}^{(O)}$, of the Pareto fronts in Fig. 11(b) and maps of the spatial distribution of the power, $\mathcal{P}_{\mathfrak{R}}(\mathbf{r})$, reflected from the EMS in (d)-(f) the region Ψ and within (g)-(i) the AoI Ω ($\Omega \subset \Psi$) when using tiles with side-length (a)(d)(g) $L = 0.25$ [m], (b)(e)(h) $L = 0.25$ [m], and (c)(f)(i) $L = 1.0$ [m].

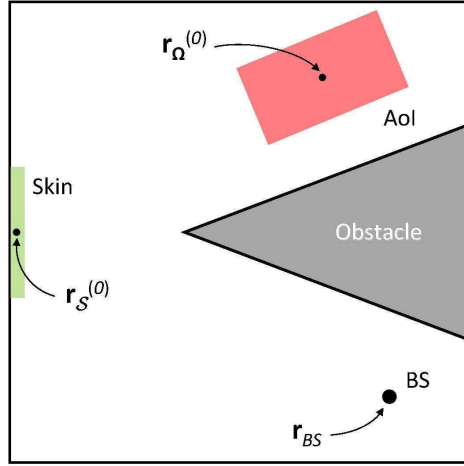
- **Figure 13.** *Numerical Validation - Complex Skin Layout - Orthogonal Incidence* ($f = 27$

[GHz], $\mathcal{S} = 15$ [m²], $L = 0.5$ [m], $N = 60$, $\Delta\Omega = 1000$ [m²], $\mathcal{P}_{th} = -70$ [dB]). Sketch of (a) the scenario and of the admissible surface \mathcal{S} along with its tile discretization and plot of (b) the iterative ($i = 100$, $i = 500$, and $i = I$) evolution of the population of the P ($P = 2 \times N$) trial solutions, $\{\mathbf{T}_i^{(p)}; p = 1, \dots, P\}$, in the space of the design objectives along with the Pareto front at convergence ($i = I$), $\{\mathbf{T}_{opt}^{(o)}; o = 1, \dots, O\}$.

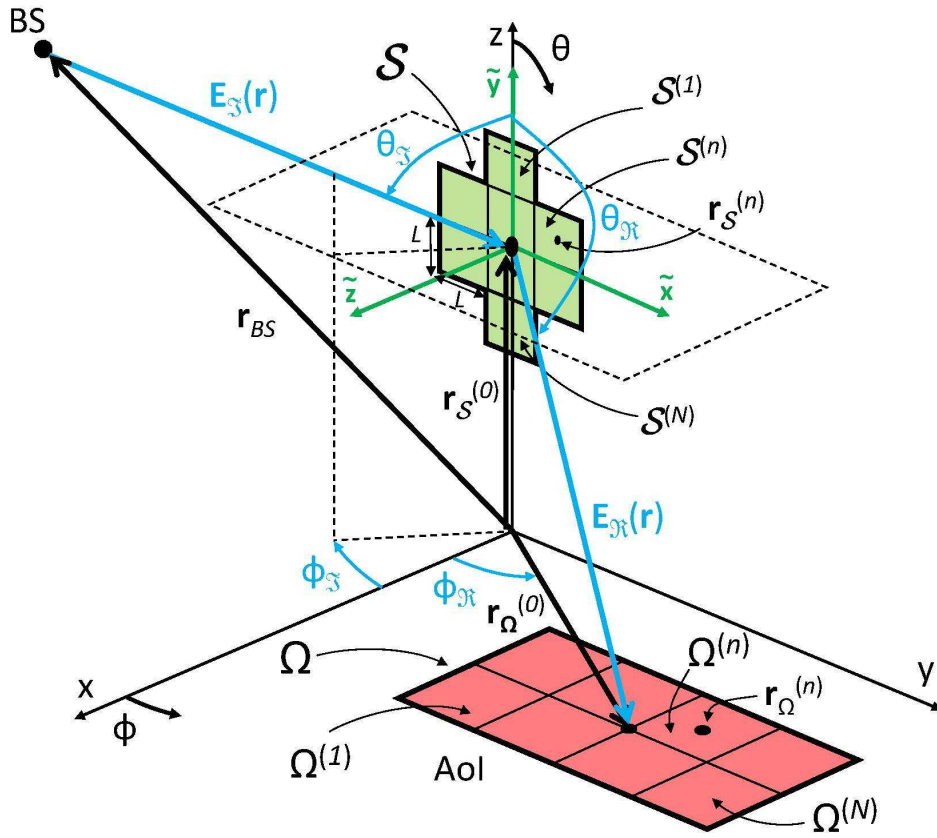
- **Figure 14.** *Numerical Validation - Complex Skin Layout - Orthogonal Incidence* ($f = 27$ [GHz], $\mathcal{S} = 15$ [m²], $L = 0.5$ [m], $N = 60$, $\Delta\Omega = 1000$ [m²], $\mathcal{P}_{th} = -70$ [dB]). Plot of (a) the *EMS* layout and of (b)(c) the corresponding spatial distributions of the power, $\mathcal{P}_{\Re}(\mathbf{r})$, reflected from the *EMS* along with (d) the coverage/connectivity maps for the O -th ($O = 31$) solution of the Pareto front in Fig. 13(b).

TABLE CAPTIONS

- **Table I.** *Numerical Validation.* Statistics of the reflected power $\mathcal{P}_{\Re}(\mathbf{r})$ within the *AoI*, Ω .



(a)



(b)

Fig. 1 - P. Rocca *et al.*, “On the Design of Modular Reflecting EM Skins ...”

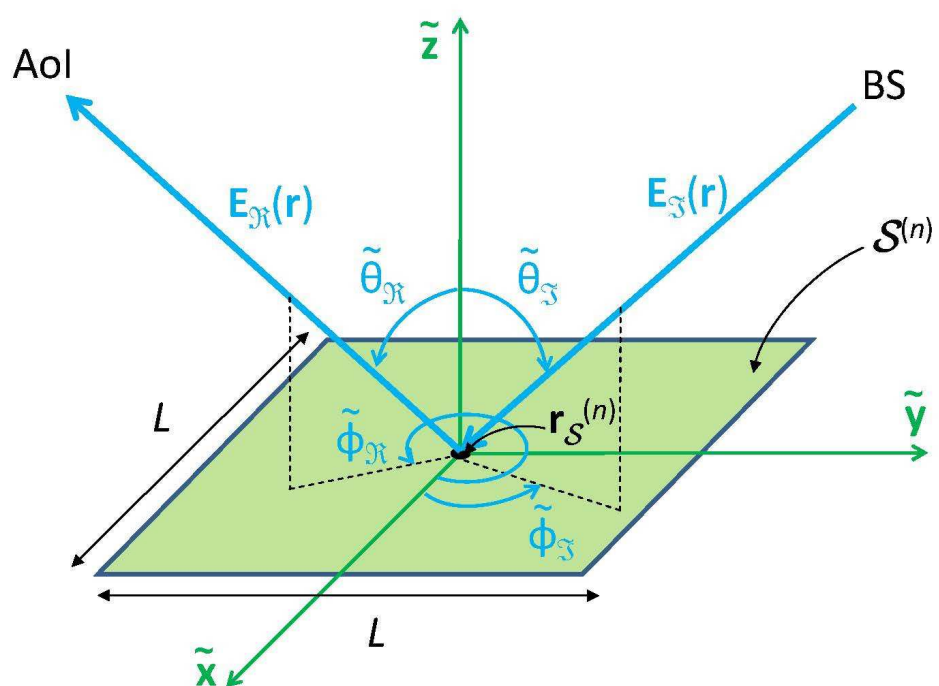
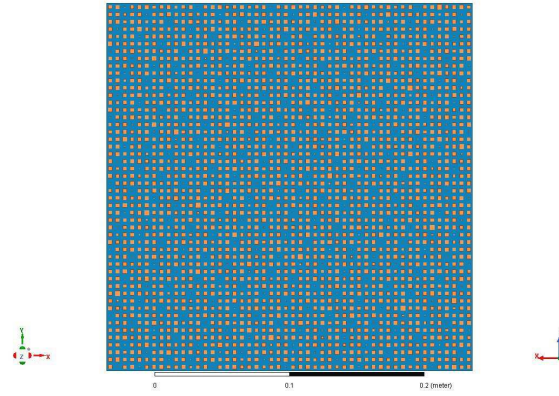
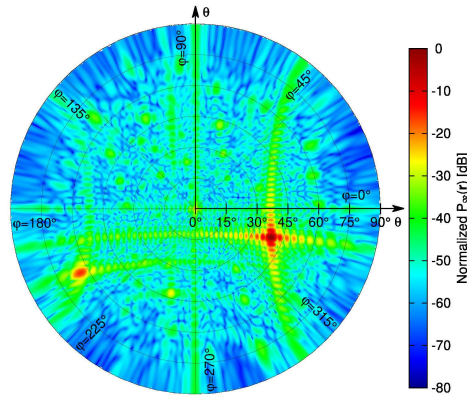


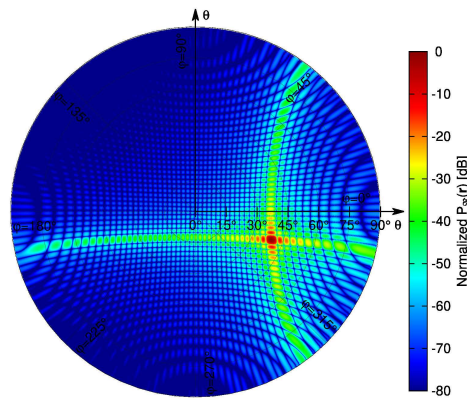
Fig. 2 - P. Rocca *et al.*, “On the Design of Modular Reflecting EM Skins ...”



(a)



(b)



(c)

Fig. 3 - P. Rocca *et al.*, “On the Design of Modular Reflecting EM Skins ...”

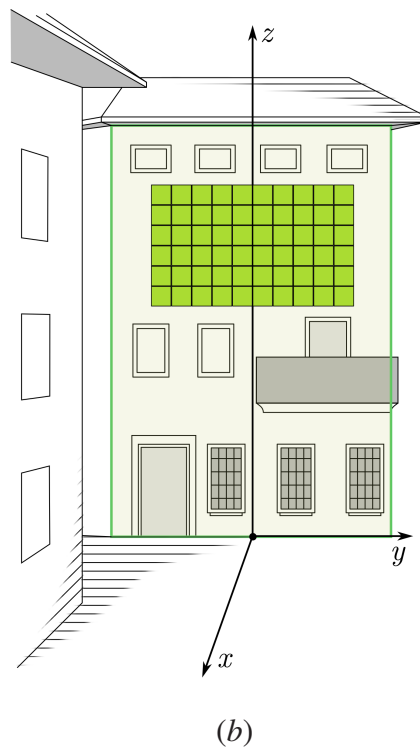
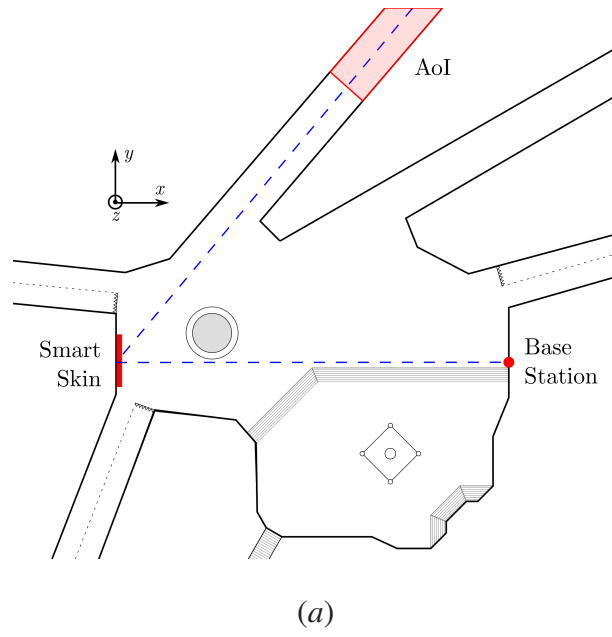


Fig. 4 - P. Rocca *et al.*, “On the Design of Modular Reflecting EM Skins ...”

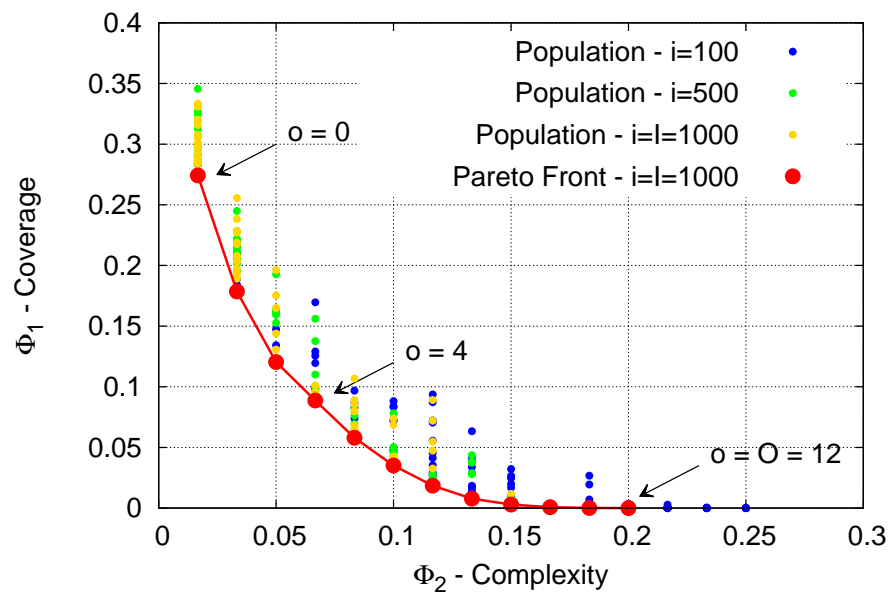
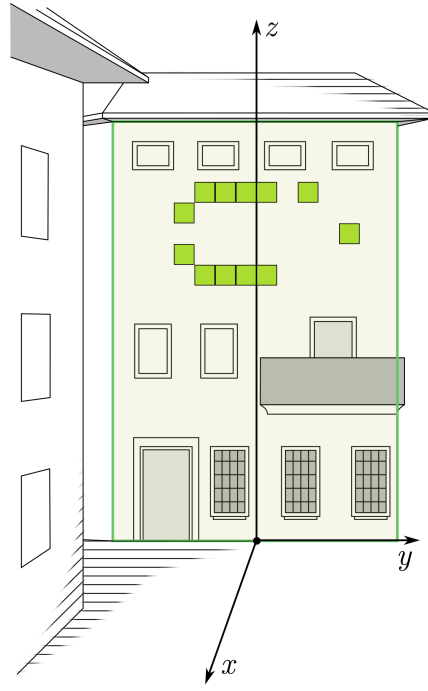
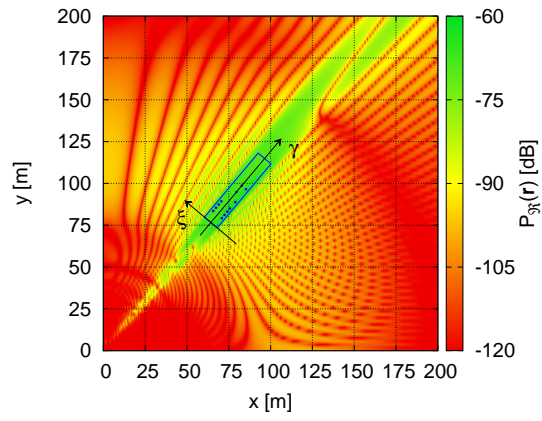


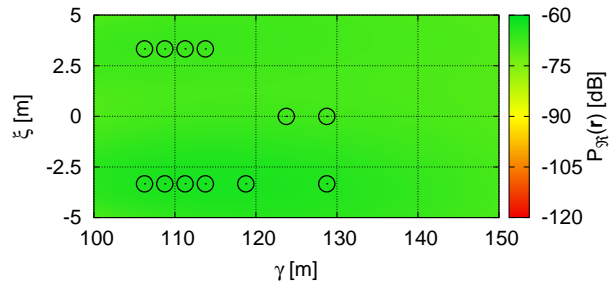
Fig. 5 - P. Rocca *et al.*, “On the Design of Modular Reflecting EM Skins ...”



(a)



(b)



(c)

Fig. 6 - P. Rocca *et al.*, “On the Design of Modular Reflecting EM Skins ...”

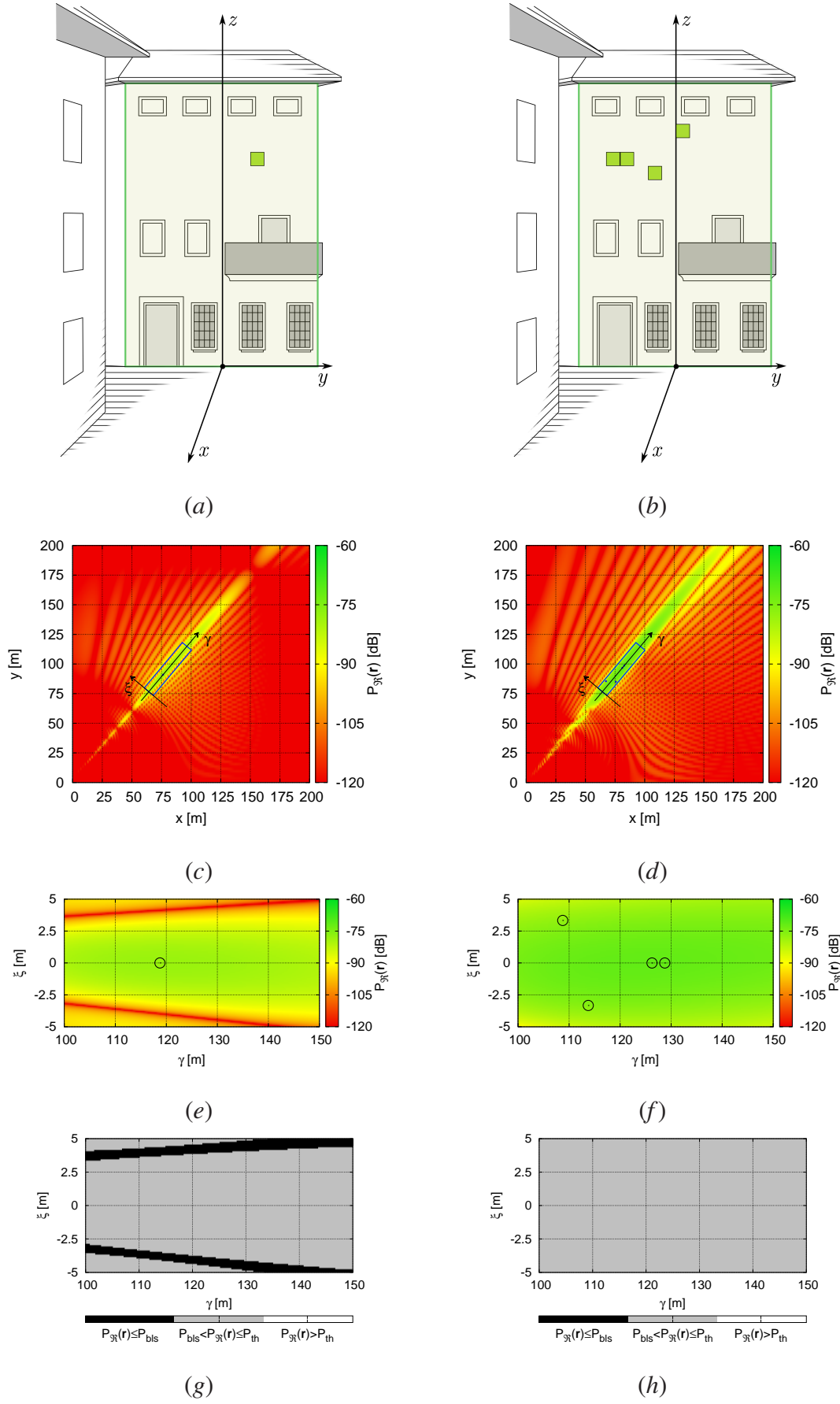


Fig. 7 - P. Rocca *et al.*, “On the Design of Modular Reflecting EM Skins ...”

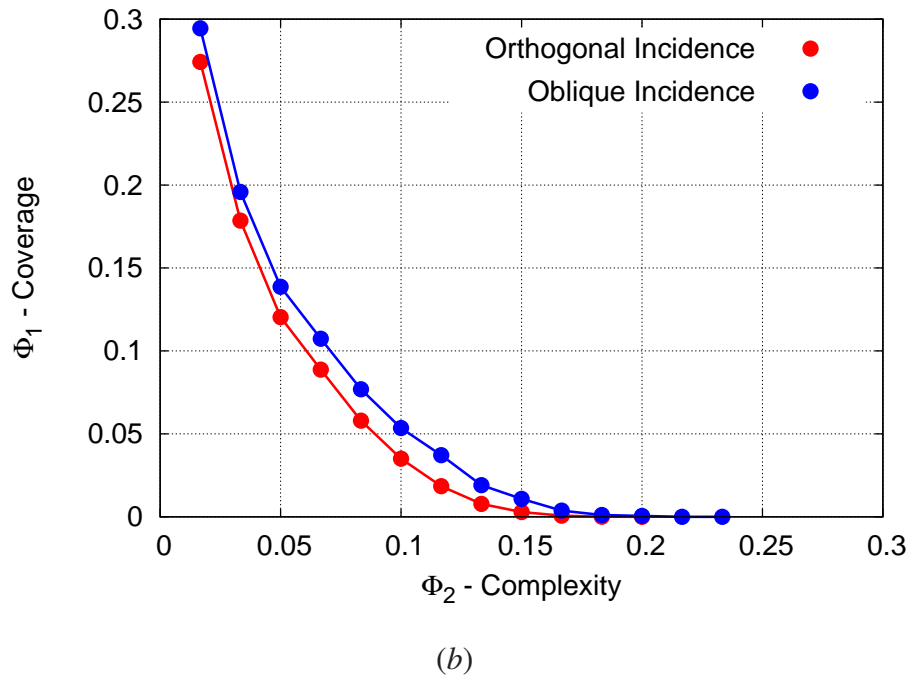
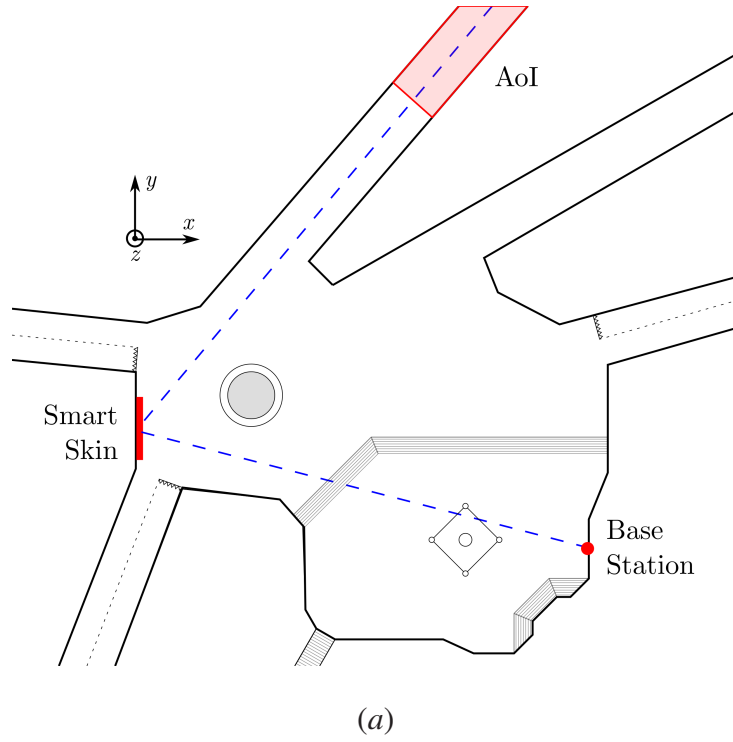
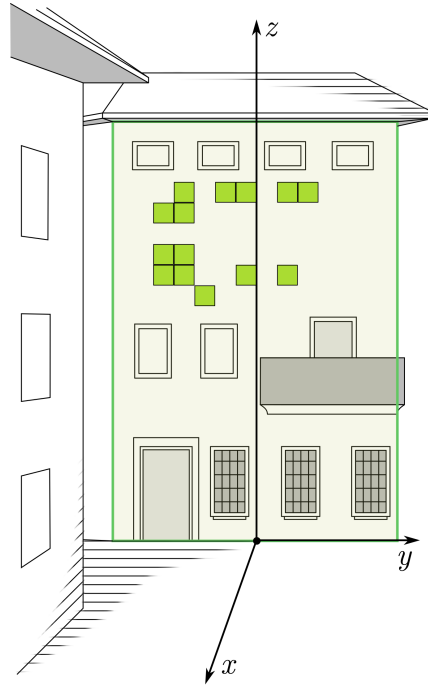
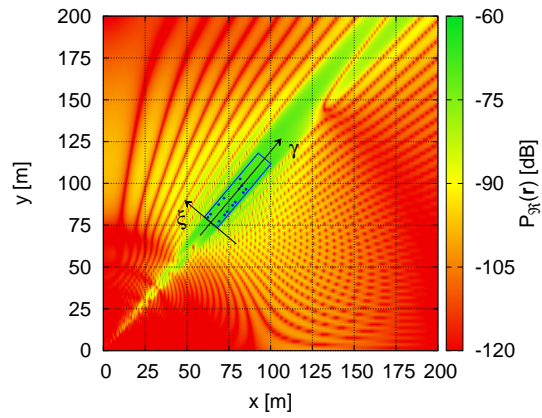


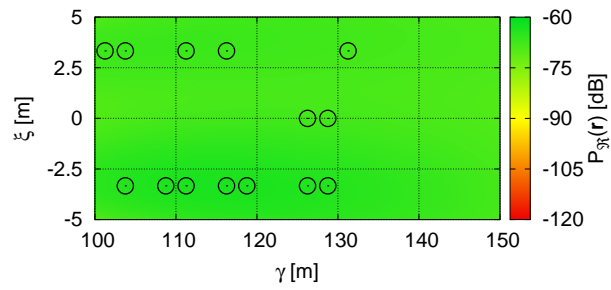
Fig. 8 - P. Rocca *et al.*, “On the Design of Modular Reflecting EM Skins ...”



(a)

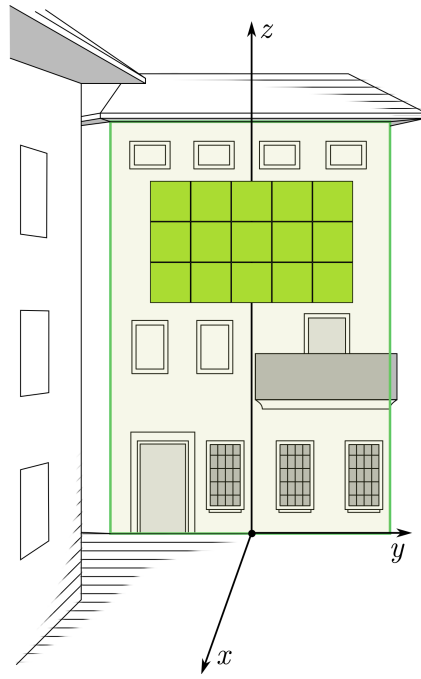


(b)

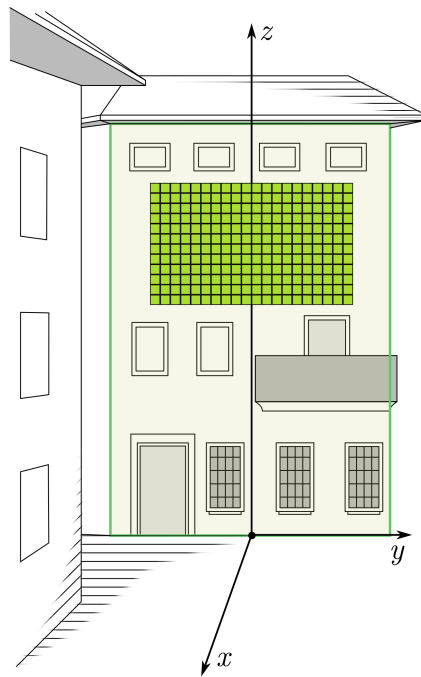


(c)

Fig. 9 - P. Rocca *et al.*, “On the Design of Modular Reflecting EM Skins ...”



(a)



(b)

Fig. 10 - P. Rocca *et al.*, “On the Design of Modular Reflecting EM Skins ...”

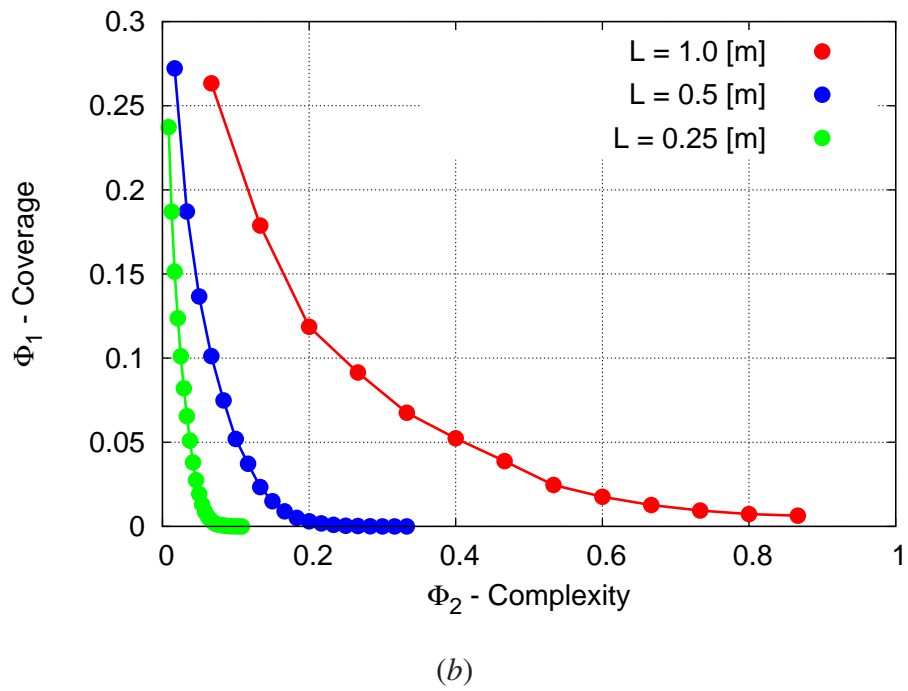
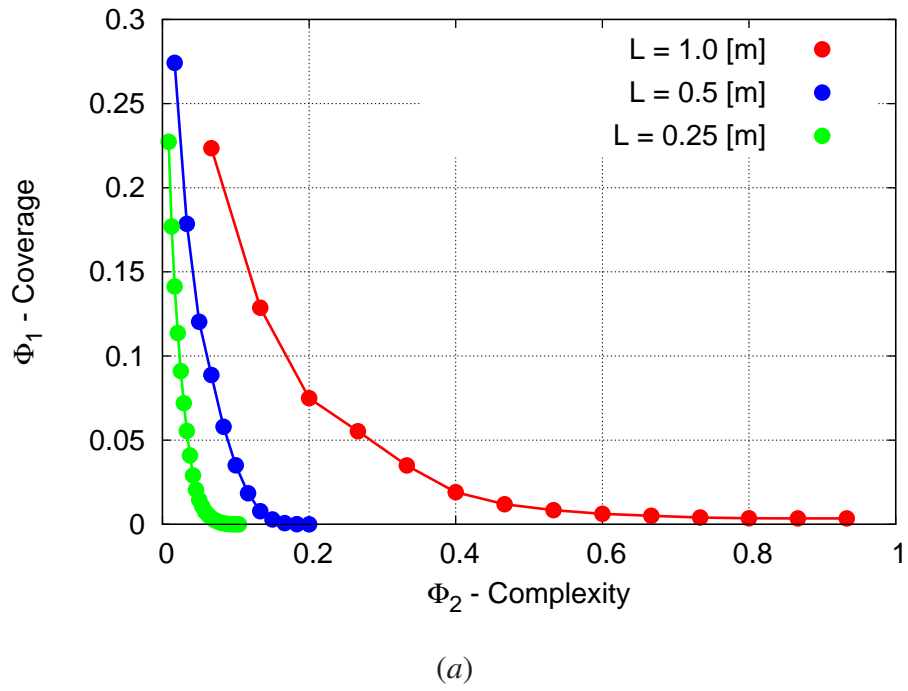
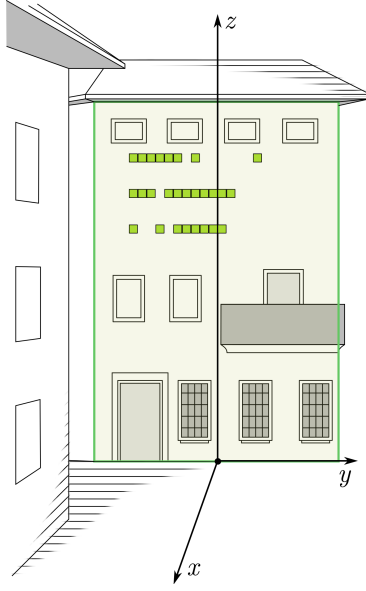
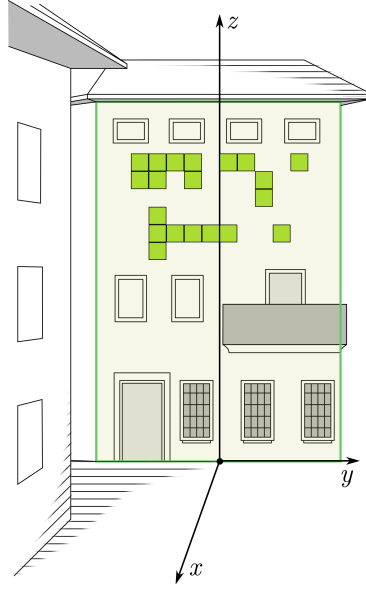


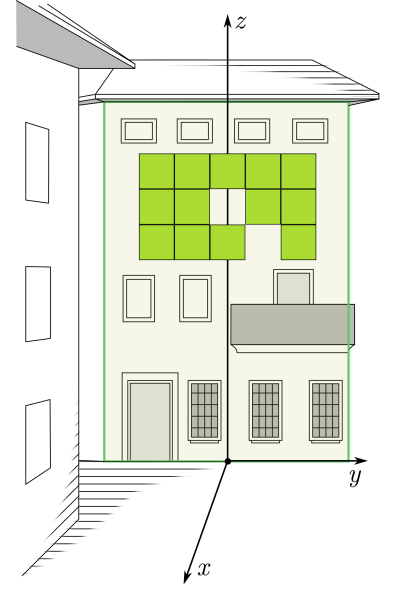
Fig. 11 - P. Rocca *et al.*, “On the Design of Modular Reflecting EM Skins ...”



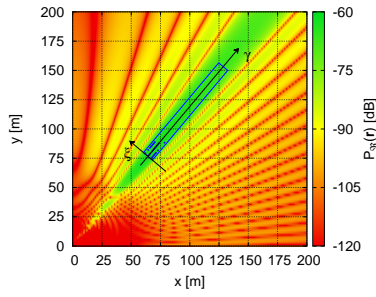
(a)



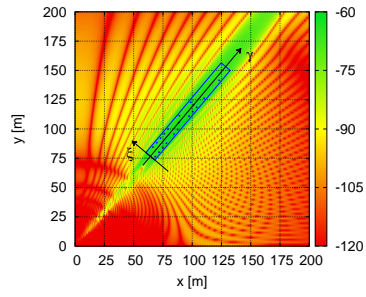
(b)



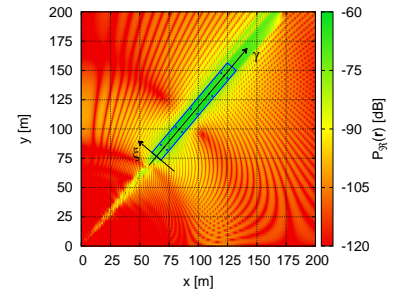
(c)



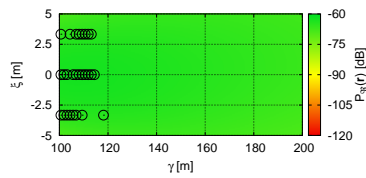
(d)



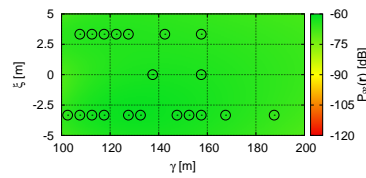
(e)



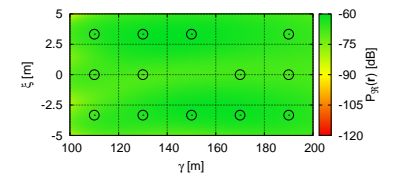
(f)



(g)



(h)

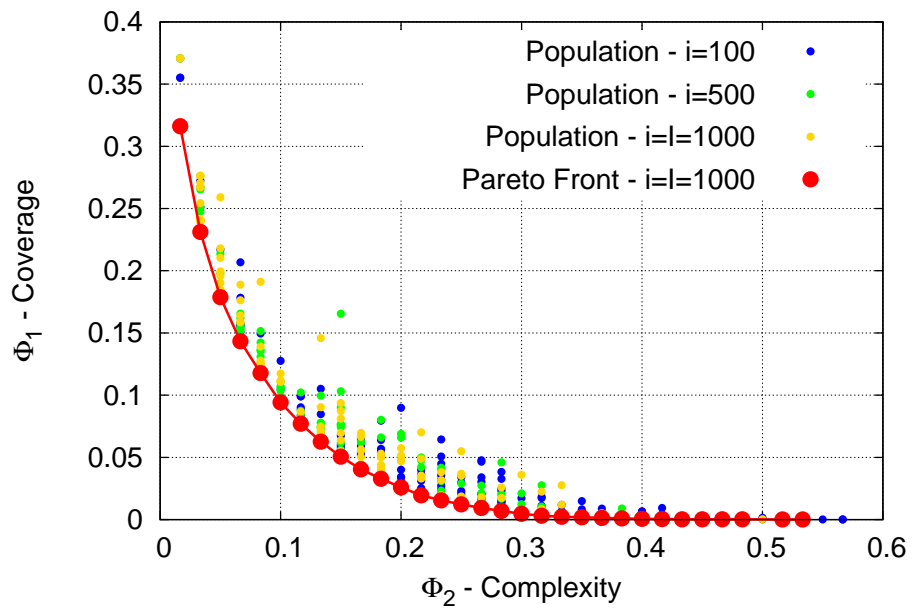


(i)

Fig. 12 - P. Rocca *et al.*, “On the Design of Modular Reflecting EM Skins ...”

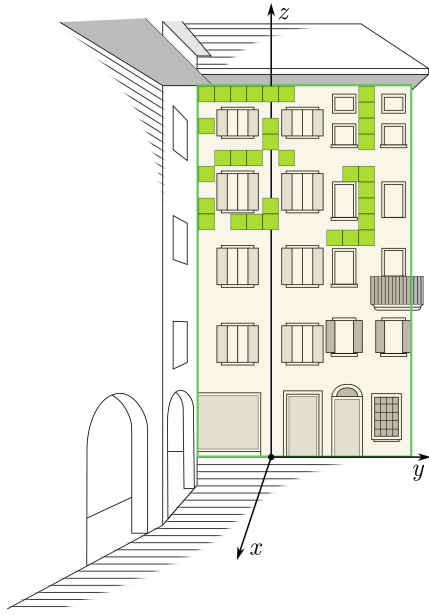


(a)

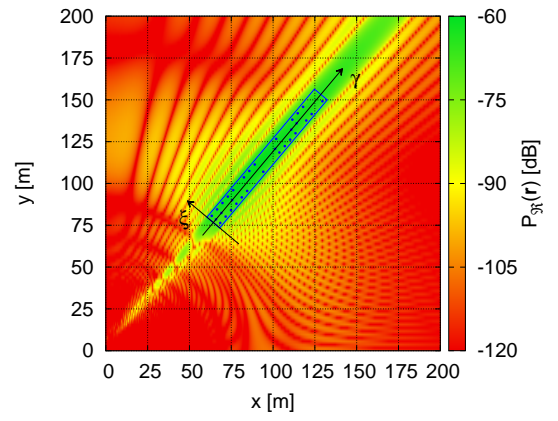


(b)

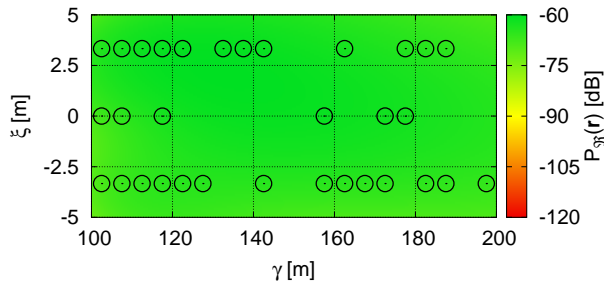
Fig. 13 - P. Rocca *et al.*, “On the Design of Modular Reflecting EM Skins ...”



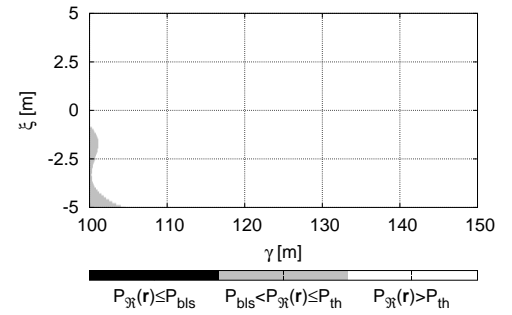
(a)



(b)



(c)



(d)

Fig. 14 - P. Rocca *et al.*, “On the Design of Modular Reflecting EM Skins ...”

	$\min_{\mathbf{r} \in \Omega} \{ E_{rx}(\mathbf{r}) ^2\} \text{ [dB]}$	$\max_{\mathbf{r} \in \Omega} \{ E_{rx}(\mathbf{r}) ^2\} \text{ [dB]}$	$\text{avg}_{\mathbf{r} \in \Omega} \{ E_{rx}(\mathbf{r}) ^2\} = \Phi_1 \text{ [dB]}$
Fig. 6(c)	-69.9	-63.0	-66.8
Fig. 7(e)	-173.9	-78.1	-84.7
Fig. 7(f)	-90.9	-71.7	-75.0
Fig. 9(c)	-69.9	-63.2	-66.9
Fig. 12(g)	-69.7	-62.5	-65.1
Fig. 12(h)	-69.7	-61.2	-64.4
Fig. 12(i)	-101.5	-60.3	-65.1
Fig. 14(c)	-73.1	-60.1	-63.5

Tab. I - P. Rocca *et al.*, “On the Design of Modular Reflecting EM Skins ...”